Science Arts & Métiers (SAM)
is an open access repository that collects the work of Arts et Métiers Institute of Technology researchers and makes it freely available over the web where possible.

This is an author-deposited version published in: https://sam.ensam.eu
Handle ID: .http://hdl.handle.net/10985/17440

To cite this version :

Rachele ALLENA, Marco SCIANNA, Luigi PREZIOSI - A Cellular Potts Model of single cell migration in presence of durotaxis - Mathematical Biosciences p.57-70 - 2016

Any correspondence concerning this service should be sent to the repository Administrator : scienceouverte@ensam.eu

A Cellular Potts Model of single cell migration in presence of durotaxis

R. Allena[a,*], M. Scianna[b], L. Preziosi[b]

[a] Arts et Metiers ParisTech, LBM/Institut de Biomecanique Humaine Georges Charpak, 151 bd de l'Hopital, 75013 Paris, France
[b] Dipartimento di Scienze Mathematiche, Politecnico di Torino, Corso Duca degli Abruzzi 24, 10129 Torino, Italy

A B S T R A C T

Cell migration is a fundamental biological phenomenon during which cells sense their surroundings and respond to different types of signals. In presence of durotaxis, cells preferentially crawl from soft to stiff substrates by reorganizing their cytoskeleton from an isotropic to an anisotropic distribution of actin filaments. In the present paper, we propose a Cellular Potts Model to simulate single cell migration over flat substrates with variable stiffness. We have tested five configurations: (i) a substrate including a soft and a stiff region, (ii) a soft substrate including two parallel stiff stripes, (iii) a substrate made of successive stripes with increasing stiffness to create a gradient and (iv) a stiff substrate with four embedded soft squares. For each simulation, we have evaluated the morphology of the cell, the distance covered, the spreading area and the migration speed. We have then compared the numerical results to specific experimental observations showing a consistent agreement.

Keywords:
Cell migration
Durotaxis
Cell polarity
Anisotropy
CPM

1. Introduction

Cell migration is a critical phenomenon occurring in several biological processes, such as morphogenesis [1], wound healing [2] and tumorogenesis [3]. It takes place in successive and cyclic steps [4] and it is triggered by specific interactions with the extracellular matrix (ECM). Actually, cell migration may occur in the absence of external signals thereby typically resulting in a random walk. However, in most situations, cells are able to sense their surrounding environment and to respond for instance to chemical (i.e., chemotaxis) [5], electrical (i.e., electrotaxis) [6] or mechanical (i.e., mechanotaxis) [7] fields or yet to stiffness gradients (i.e., durotaxis) [8,9]. The latter mechanism consists of the cell preferential crawling from soft matrix substrates to stiffer ones, even in the absence of any additional directional cues [10,11]. By forming local protrusions (i.e., pseudopodia), the cells are in fact able to probe the mechanical properties of the surrounding environment and to more strongly adhere over stiff regions. Additionally, such behavior results in a substantial reorganization of the intracellular cytoskeleton. In fact, over soft substrates cells typically show an unstable and isotropic distribution of actin filaments, which are poorly extended and radially oriented, whereas over stiff substrates cell morphology is more stable and exhibits significant spreading and often anisotropic arrangements of actin filaments in the direction of migration (i.e., polarization) [12–16].

Although several computational models have been proposed in literature to investigate single cell migration, only few of them deal with durotaxis. Among others, it is worth to cite the work by Moreo et al. [17] who proposed a continuum approach based on an extension of the Hill's model for skeletal muscle behavior to investigate cell response on two-dimensional (2D) substrates. They showed, in agreement with experimental observations, that cells seem to have the same behavior when crawling on stiffer substrate and on pre-strained substrates. Harland et al. [18] instead represented a cell as a collection of stress fibers undergoing contraction and birth/death processes and showed that on stiff substrates cells exhibit durotaxis and stress fibers significantly elongate. Dokukina and Gracheva [19] developed a 2D discrete model of a viscoelastic fibroblast cell using a Delaunay triangulation. At each node the balance of the forces was determined by the contributions i) of the frictions between the cell and the substrate, ii) of a passive viscoelastic force and iii) of an intrinsic active force. The authors then evaluated cell behavior over a substrate with a rigidity step in good agreement with specific experimental observations. In fact, they found that the cell preferentially moves on the stiffer substrate and turns away from the soft substrate as reported by [8]. Stefanoni et al. [20] proposed a finite element approach able to account for the local mechanical properties of the underneath substrate and to analyze selected cell migratory determinants on two distinct configurations: an isotropic substrate and a biphasic substrate (which consists of two adjacent isotropic regions with different mechanical properties). Trichet et al. [14] employed instead the active gel theory to demonstrate that cells preferentially migrate over stiff substrates founding an optimal range of rigidity for

* Corresponding author. Tel.: +33 1 44 24 61 18; fax: +33 1 44 24 63 66.
E-mail address: rachele.allena@ensam.eu (R. Allena).

http://dx.doi.org/10.1016/j.mbs.2016.02.011

a maximal efficiency of cell migration. Further, in [21] a vertex-based approach (i.e., the so-called Subcellular Element Model, SCE) was set to represent intracellular cytoskeletal elements as well as their mechanical properties. In particular, the dynamics of such subcellular domains were described by Langevin equations, which account for a weak stochastic component (i.e., that mimic cytoplasmic fluctuations) and elastic responses (i.e., modeled by generalized Morse potentials) to both intracellular and intercellular biomechanical forces. The same method was successfully applied in [22] for modeling substrate-driven bacteria locomotion. Finally, in Allena and Aubry [23] a 2D mechanical model was proposed to simulate cell migration over an heterogeneous substrate including slipping regions and to show that over softer regions the cell slows down and is less efficient.

In the present work, we describe a Cellular Potts Model (CPM, developed in [24,25] and reviewed in [25–29]), which is a lattice-based stochastic approach employing an energy minimization philosophy, to reproduce single cell migration over flat substrates with different rigidity. In particular, we test four configurations: (i) a substrate including a soft and a stiff region, (ii) a soft substrate including two parallel stiff stripes, (iii) a substrate made of successive stripes with increasing stiffness to create a gradient and (iv) a stiff substrate with four embedded soft squares. For each scenario, we analyze cell behavior in terms of morphology, distance covered, spreading/adhesive area and migration speed in order to capture the essential mechanisms of durotaxis. The computational outcomes are then compared with specific experimental observations taken from the existing literature.

The rest of this paper is organized as follows. In Section 2, we clarify the assumptions on which our approach is based and present the model components. The simulation results are then shown in Section 3. Finally, a justification of our model choices as well as a discussion on possible improvements is proposed in Section 4. Additionally, the article is equipped with an Appendix that deals with statistics and parameter estimates.

2. Mathematical model

The cell-substrate system is represented using a CPM environment [24,25]. The simulation domain is a three-dimensional (3D) regular lattice $\Omega \in R^3$ constituted by identical closed grid sites, which are identified by their center $\boldsymbol{x} \in R^3$ and labeled by an integer number $\sigma(\boldsymbol{x}) \in N$ (which can be interpreted as a degenerate spin) [30,31]. The boundary of a generic site $\boldsymbol{x}$, one of its neighbors and its overall neighborhood are defined as $\partial\boldsymbol{x}$, $\boldsymbol{x}'$ and $\Omega'_{\boldsymbol{x}}$, respectively. Subdomains with identical label σ form discrete objects Σ_σ (with border $\partial\Sigma_\sigma$), which have an associated type $\tau(\Sigma_\sigma)$. In the case of our interest, $\tau = M$ stands for the medium, $\tau = C$ for the cells and $\tau = S_i$ for the ith type of substrate. In this respect, we anticipate that each type of matrix region will differ for stiffness and therefore for adhesive affinity with moving individuals.

Cell dynamics result from an iterative and stochastic reduction of the energy of the overall system, given by a Hamiltonian H (units: kg m^2/s^2), whose expression will be clarified below. The employed algorithm is a modification of the Metropolis method for Monte Carlo–Boltzmann dynamics [24,32], which is particularly suitable to simulate the exploratory behavior of biological individuals as cells. Procedurally, at each time step t of the algorithm, called Monte Carlo Step (MCS), a randomly chosen lattice site $\boldsymbol{x}_{source}$ belonging to a cell tries to allocate its spin $\sigma(\boldsymbol{x}_{source})$ to one of its unlike neighbors $\boldsymbol{x}_{\text{target}} \in \Omega'_x$, which is also randomly selected. Then, the net energy difference ΔH due to the proposed change of system configuration is calculated as

$$\Delta H|_{\sigma(\boldsymbol{x}_{source})\to\sigma(\boldsymbol{x}_{\text{target}})} = H_{(\text{after spin copy})} - H_{(before\text{spin copy})} \tag{1}$$

The trial spin update is finally validated by a Boltzmann-like probability function defined as

$$P[\sigma(\boldsymbol{x}_{source}) \to \sigma(\boldsymbol{x}_{\text{target}})](t) = \min\left\{1, e^{-\frac{\Delta H}{T_C}}\right\} \tag{2}$$

where t is the actual MCS and $T_C \in R_+$ is a Boltzmann temperature, that has been interpreted in several ways by CPM authors (see [33] for a comment on this aspect). However, we here opt to give T_C the sense of a cell intrinsic motility (i.e., agitation rate), following the approach in [25]. Finally, it is useful to underline that the matrix substrates are considered fixed and immutable.

As seen, the simulated system evolves to iteratively and stochastically reduce its free energy, which is defined by a Hamiltonian function H which, for any given time step t, reads

$$H(t) = H_{adhesion}(t) + H_{shape}(t) \tag{3}$$

$H_{adhesion}(t)$ is deduced from the Steinberg's Differential Adhesion Hypothesis (DAH) [24,34] and is due to the adhesion between cells and extracellular components (i.e., the medium or a given type of substrate). In particular, it reads

$$H_{adhesion}(t) = H_{adhesion}(t) = \sum_{(\partial\boldsymbol{x}\in\partial\Sigma_\sigma)\cap(\partial\boldsymbol{x}'\in\partial\Sigma_{\sigma'})} J_{\tau(\Sigma_{\sigma(\boldsymbol{x})}),\tau(\Sigma_{\sigma'(\boldsymbol{x}')})} \tag{4}$$

with $\boldsymbol{x}$ and $\boldsymbol{x}'$ two neighboring sites and Σ_σ and $\Sigma_{\sigma'}$ two neighboring objects (with borders $\partial\Sigma_\sigma$ and $\partial\Sigma_{\sigma'}$, respectively). $J_{\tau(\Sigma_{\sigma(\boldsymbol{x})}),\tau(\Sigma_{\sigma'(\boldsymbol{x}')})} \in R_+$ are constant and homogeneous binding forces per unit area. They are symmetric with respect to their indices and can be specified as follows:

- $J_{C,M}$ is the adhesive strength between the cells and the collagenous medium which is constituted by a mixture of soluble adhesive ligands (i.e., carbohydrate polymers and non-proteoglycan polysaccharides) and water solvent;
- J_{C,S_i} gives the adhesive strength between the cells and ith type of substrate. Recalling the minimization theory of the CPM, we assume that the stiffer the substrate i, the lower the corresponding value J_{C,S_i} (i.e., the higher the adhesion between the cells and the ith type of substrate). This is a pivotal hypothesis of our approach: it is consistent since it has been widely demonstrated in the experimental literature that cells generate higher traction forces and generate more stable focal adhesion points when migrating over stiffer substrates [16,35–38].

$H_{shape}(t)$ defines the geometrical attributes of each cell Σ_σ, which are written as elastic potentials as it follows:

$$\begin{aligned} H_{shape}(t) &= H_{volume}(t) + H_{surface}(t) \\ &= \sum_{\Sigma_\sigma} [\kappa_{\Sigma_\sigma}(\nu_{\Sigma_\sigma}(t) - V_C)^2 + \nu_{\Sigma_\sigma}(t)(s_{\Sigma_\sigma}(t) - S_C)^2] \end{aligned} \tag{5}$$

where$\nu_{\Sigma_\sigma}(t)$ and $s_{\Sigma_\sigma}(t)$ are the actual volume and surface of the cell Σ_σ, whereas V_C and S_C the corresponding cell characteristic measures in the initial resting condition.κ_{Σ_σ} and $\nu_{\Sigma_\sigma}(t)$ are instead two mechanical moduli in units of energy. The former is linked to volume changes and, assuming that cells do not significantly grow during migration, is considered constant with a high value (i.e., $\kappa_{\Sigma_\sigma} = \kappa_C \gg 1$) for any individual Σ_σ. The latter refers to the rigidity of a cell. As we will explain in details later on, for each cell Σ_σ, ν_{Σ_σ} is assumed to depend on the underneath type of substrate. In particular, each cell decreases its initially high (i.e., $\gg$1) rigidity, thereby being more able to deform, if it comes in contact with a stiff substrate. This assumption is consistent with experimental observations on the fact that cell contact with stiff matrix regions activate downstream intracellular pathways resulting in acto-myosin dynamics and therefore in cytoskeletal remodeling [8,39]. More specifically, it seems that certain cells have a binary sensor at their membrane junction sites that allows them

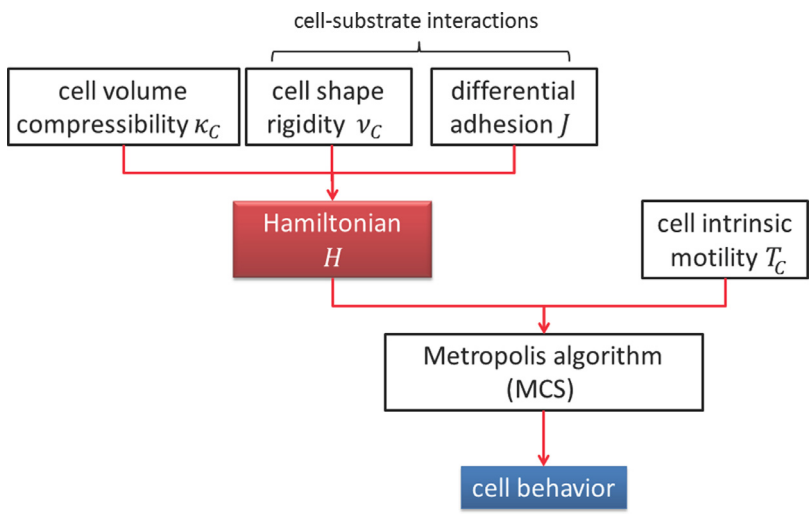

Fig. 1. Cell behavior is determined by a modified Metropolis algorithm, which is based on a iterative and stochastic minimization of the cell–matrix system energy, defined by a Hamiltonian functional H. In particular, it includes energetic contributions for cell geometrical attributes and cell-substrate adhesive affinity. A Boltzmann-like law finally controls the likelihood of the acceptance of domain configuration updates, which is further biased by the intrinsic cell motility, established by parameter T_C.

Table 1
Main parameters of the model.

Parameter	Description	Value	Unit	Reference(s)
V_C	Initial/target cell volume	16×10^3	μm^3	[46]
S_C	Initial/target cell surface	3.8×10^3	μm^2	[46]
T_C	Motility of the cell	50×10^{-27}	$kg\ m^2/s^2$	Sensitivity analysis (see Fig. 10)
κ_C	Compressibility of cell volume	25×10^{-9}	$kg/s^2\ m^4$	Sensitivity analysis in [80,89]
ν_C	Cell intrinsic rigidity	25×10^{-3}	$kg/s^2\ m^2$	Sensitivity analysis in [57,68,80,89]
ν_t	Threshold value of cell rigidity	10×10^{-3}	$kg/s^2\ m^2$	Parameter analysis (Appendix A.3)
$J_{C,M}$	Cell-medium adhesive strength	25×10^{-15}	kg/s^2	Parameter analysis (Appendix A.3)
J_{soft}	Adhesive strength between cells and the softest substrate	25×10^{-15}	kg/s^2	Sensitivity analysis (see Fig. 10)
J_{stiff}	Adhesive strength between cells and the stiffest substrate	1×10^{-15}	kg/s^2	Parameter analysis (Appendix A.3)

to switch from a relaxed and rounded morphology, when the substrate is softer than the cell's elastic modulus [39–43], to a fan-shaped morphology with abundant stress fibers, when the substrate is stiffer or as stiff as the cell itself [39]. Further, it has been shown that cells tend to isotropically and poorly spread on soft substrates, whereas they form pseudopodia randomly distributed along the membrane on stiff substrates, resulting in a significant anisotropic spreading [16]. In this respect, according to several experimental observations [16,35–38,44], there exists a linear relationship between the adhesion forces exerted by the cell on the substrate and the spreading area of the cell. More specifically, the larger the contact area between the cell and the substrate, the higher the number of focal adhesion points that can be established. Nonetheless, the sequence of events is still unclear and two main processes may occur when a cell is seeded on a stiff substrate [45]:

(i) the cell adheres because of the stiffness of the substrate, then it significantly spreads;
(ii) the cell spreads because of the stiffness of the substrate, then it more strongly adheres.

Such uncertainty is the reason why in the present model both the adhesive parameters and the cell rigidity directly depend on the substrate stiffness, but are independent from each other.

The main components and the scales involved in the proposed model are summarized in the diagram in Fig. 1. Finally, all the parameters of the simulations are reported in Table 1, while the Appendix provides a careful explanation of how they have been estimated.

3. Numerical simulations

The characteristic size of each lattice site is $4\,\mu m$ and the geometrical domain Ω is a $70 \times 70 \times 30$ regular grid ($280\,\mu m \times 280\,\mu m \times 120\,\mu m$) with no-flux boundary conditions in all directions. This choice mimics the situation of a delimited experimental device, where cells are not able to overcome the physical barriers. All our CPM cells are initially a hemisphere of a radius of $20\,\mu m$, whose initial position will be specified for each simulation setting. A MCS is set to correspond to 2 s of actual unit of time (see the Appendix for a comment on this aspect), which results in simulations covering time intervals between 16 min to 5.5 h. This choice enables cells to migrate over sufficiently long paths in order to compare numerical results and proper experimental observations. We have tested several cell–matrix settings, which are presented in the followings. The resulting simulations were performed on a modified version of the open source package CompuCell3D (downloadable at www.compucell3d.org). In particular, a Phyton script was specifically developed to account for substrate-dependent cell rigidity.

3.1. Cells preferentially crawl over stiff substrates

We first consider a substrate split into a soft and a stiff region, i.e., $\tau = S_1$ and $\tau = S_2$ (see Fig. 2a). A cell Σ_1 is then seeded at the center of the substrate and it is allowed to move for 500 MCS (approximately 16 min). The rigidity of Σ_1, ν_{Σ_1}, has initially a high value $\nu_{\Sigma_1} = \nu_C = 25 \times 10^{-3}\ kg/s^2\ m^2$. However, it is allowed to decrease, of $10^{-3}\ kg/s^2\ m^2$ for MCS until a threshold value ν_t equal to

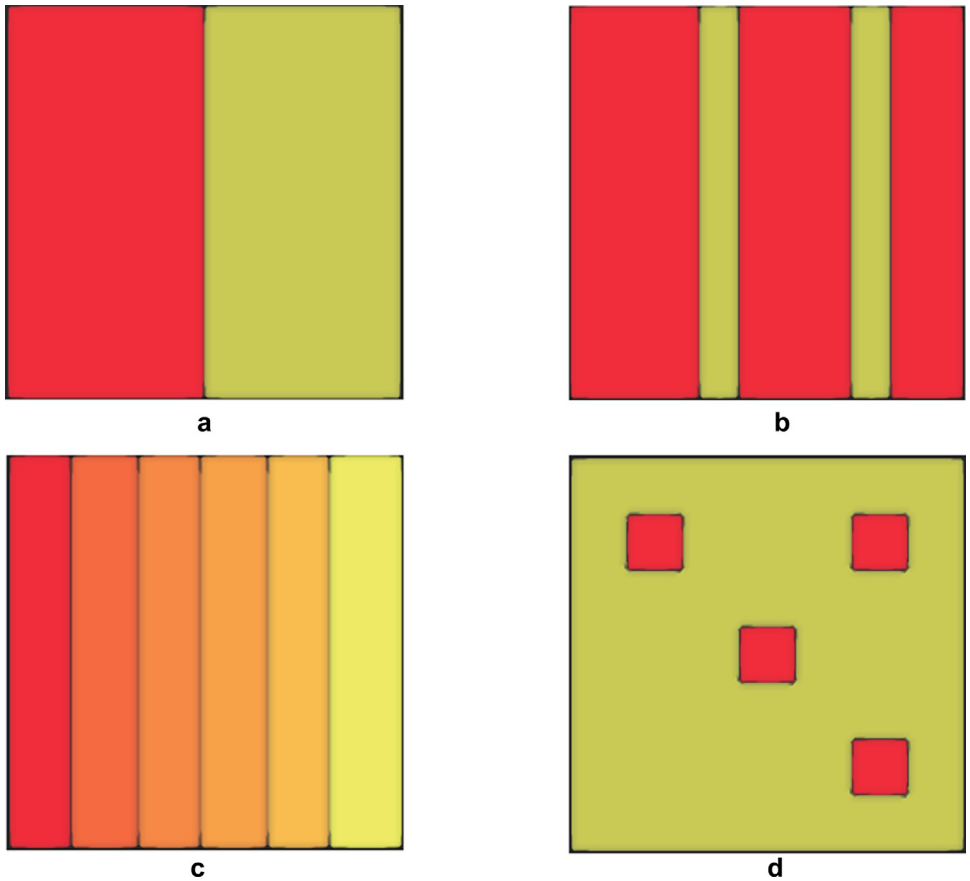

Fig. 2. Snapshots of the tested substrate configurations: (a) soft (red: τ_{S_1} with $J_{C,S_1} = 25\times10^{-15}$ kg/s^2) and stiff (yellow: τ_{S_2} with $J_{C,S_2} = 1\times10^{-15}$ kg/s^2) substrates, (b) soft (red: τ_{S_1} with $J_{C,S_1} = 25 \times 10^{-15}$ kg/s^2) substrate with two stiff (yellow: τ_{S_2} with $J_{C,S_2} = 1 \times 10^{-15}$ kg/s^2) stripes, (c) sequence of stripes with different stiffness (red: τ_{S_1} with kg/s $J_{C,S_1} = 25 \times 10^{-15}$, dark orange:$\tau_{S_2}$ with $J_{C,S_2} = 20 \times 10^{-15}$ kg/s^2, orange: τ_{S_3} with $J_{C,S_3} = 15\times10^{-15}$ kg/s^2, light orange: τ_{S_4} with $J_{C,S_4} = 10\times10^{-15}$ kg/s^2, dark yellow: τ_{S_5} with $J_{C,S_5} = 5 \times 10^{-15}$ kg/s^2, yellow: τ_{S_6} with $J_{C,S_6} = 1 \times 10^{-15}$ kg/s^2), (d) stiff (yellow: τ_{S_2} with $J_{C,S_2} = 1 \times 10^{-15}$ kg/s^2) substrate with embedded soft (red: τ_{S_1} with $J_{C,S_1} = 25 \times 10^{-15}$ kg/s^2) squares. (For interpretation of the references to colour in this figure legend, the reader is referred to the web version of this article.)

10^{-2} kg/s^2 m^2, while the cell is in contact with the stiff region S_2, thereby leading to a flattening of the initially rigid cellular hemisphere. In mathematical terms, we indeed have that

$$\nu_{\Sigma_1}(t) = \begin{cases} \max(\nu_{\Sigma_1}(t-1) - 10^{-3}; \nu_t) \\ \quad \text{if } \exists(\boldsymbol{x}, \boldsymbol{x}' \in \Omega'_{\boldsymbol{x}}) : \boldsymbol{x} \in \Sigma_1 \text{ and } \boldsymbol{x}' \in S_2; \\ \nu_{\Sigma_1}(t-1) \quad \text{else}, \end{cases} \tag{6}$$

for each MCS.

We then study how cell behavior is affected by variations in the ratio between the adhesive affinity of the cell with either the soft or the stiff substrate region. In particular, we keep fixed $J_{C,S_1} = J_{soft} = 25 \times 10^{-15}$ kg/s^2 while decreasing the value of J_{C,S_2} from 25×10^{-15} kg/s^2 to 1×10^{-15} kg/s^2 (which is equal to J_{stiff}, the lowest value consistent with the case of our interest, see the Appendix). As summarized in Fig. 3c, when J_{C,S_2} decreases, the cell is biased to crawl toward the stiff domain, as it is confirmed by the plot of the trajectories of its center of mass deriving from independent simulations. In fact, over a period of 500 MCS (≈16 min), the cell randomly moves around the substrate center when $\frac{J_{C,S_1}}{J_{C,S_2}}=1$ (Fig. 3a) while, when $\frac{J_{C,S_1}}{J_{C,S_2}}=25$, the cell trajectories dramatically shift over the stiff part of the substrate (Fig. 3b). Our numerical results are sustained and consistent with the experimental observations according to which cells (i.e., fibroblasts, smooth muscle cells, Mesenchymal Stem Cells (MSCs)) crawl from soft (1–5 kPa) to stiff (34–80 kPa) substrates (i.e., gels or polyacrylamide sheets) [9–11,46]. Notably during motion toward the stiff substrate, our CPM cell is also allowed to increase its remodeling ability, as its rigidity ν_{Σ_1} progressively decreases upon contact with substrate S_2, according to Eq. (6). In this respect, a further set of simulations evaluates cell morphological differences due to the underneath type of substrate. Keeping the same domain as in Fig. 2a, two cells, i.e., Σ_1 and Σ_2, are initially seeded in the middle of the soft and the stiff regions, respectively. The rigidity of the two cells is then regulated by Eq. (6). As reproduced in Fig. 4 (in particular, panel (a) represents the final cell morphologies as resulted from a single representative simulation, whereas panel (b) gives the mean final cell morphologies, as the plain ellipsoids derive from an interpolation procedure of the cell adhesive areas coming from independent simulations, see the Appendix for further details), both individuals do not significantly move across the domain during a time lapse of 500 MCS (approximately 16 min). However, the adhesive area of the cell located over the soft region is almost 30% lower than the adhesive area of the cell that crawls over the stiff substrate (Fig. 4c). Such a cell behavior is consistent with the experimental data by Lo and co-workers on 3T3 fibroblasts cultured on flexible polyacrylamide sheets coated with type I collagen, where a transition in rigidity was introduced by a discontinuity of the bis-acrylamide cross-linker, that resulted in two substrate regions with Young's modulus equal to either 14 kPa and 30 kPa [46]. In particular, on one hand, the value of the adhesive area of our CPM cell seeded on the soft substrate is not surprisingly similar to the corresponding data by Lo and co-workers [46], since we used such an experimental quantification for our parameter estimate (see the Appendix). On the other hand, the adhesive area of the CPM cell seeded on the stiff region is instead a completely independent and

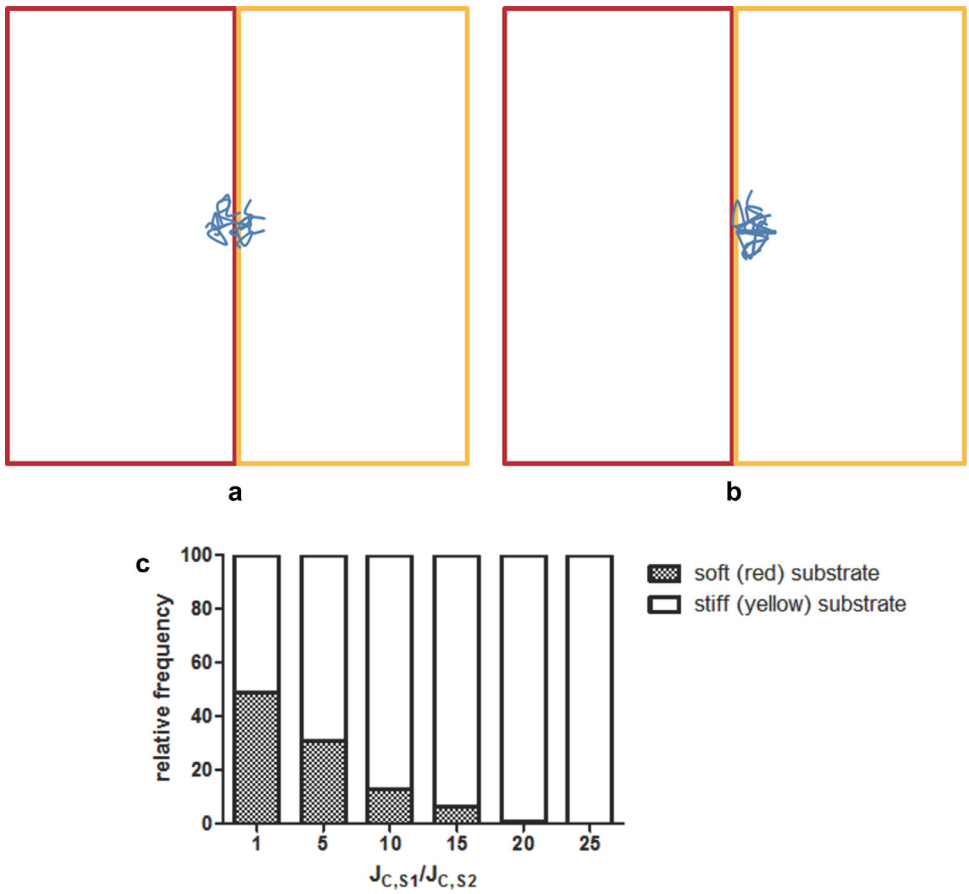

Fig. 3. Simulation for a substrate with soft (red) and stiff (yellow) regions. As the ratio $\frac{J_{C,S_1}}{J_{C,S_2}}$, increases, the cells are typically biased to migrate toward the stiff region (c). This is also confirmed by the trajectories of the cell center of mass, which are relatively close to the center of the substrate when $\frac{J_{C,S_1}}{J_{C,S_2}}=1$ (a), whereas they are substantially shifted on the stiff region when $\frac{J_{C,S_1}}{J_{C,S_2}}=25$ (b). (For interpretation of the references to colour in this figure legend, the reader is referred to the web version of this article.)

self-emerging model outcome: therefore its consistency with the measurements by Lo and colleagues [46] is relevant point of our work.

3.2. Stiff versus soft substrate in the presence of an external cue

For the second series of simulations we consider again a domain split into a soft ($\tau = S_1$ such as $J_{C,S_1} = J_{soft} = 25 \times 10^{-15}$ kg/s^2) and a stiff ($\tau = S_2$ such as $J_{C,S_2} = J_{stiff} = 1 \times 10^{-15}$ kg/s^2) region, but an additional external potential is introduced. This results in an imposed artificial bias in the spin flip rate that is able to affect the direction of cell migration. Entering more in details, the expression of the Hamiltonian function presented in Eq. (3) is modified as it follows

$$H(t) = H_{adhesion}(t) + H_{shape}(t) + H_{potential} \tag{7}$$

where $H_{potential} = -v_{ext}(\boldsymbol{x}'_{\text{target}} - \boldsymbol{x}_{source})$ and v_{ext} is a vector whose components determine the direction of the potential and whose modulus gives the relative importance in the overall system energy. For the sake of simplicity, we assume that the potential is constant in time and homogeneous throughout the entire domain. As we will see later, it is in fact an artificial term that simply helps cells to maintain a sustained directional movement. In this respect, what is relevant is only its modulus, i.e., $|\boldsymbol{v}_{ext}|$. We then test two configurations:

(a) a cell Σ_1 placed at the south-east corner and the external potential directed toward the north-west corner;

(b) the same cell Σ_1 placed at the south-west corner of the substrate and the external potential directed toward the north-east corner.

In both cases, we set $|\boldsymbol{v}_{ext}| = 7 \times 10^{-21}$ kg m/s^2, which results in plausible cell velocities (see later) and the simulations last 10,000 MCS (approximately 5.5 h). Further, cell rigidity is again regulated by Eq. (6).

In system configuration (a) (see Movie 1 and Fig. 5a), the external cue guides the cell toward the north-west corner of the domain. In particular, when a part of the cell comes into contact with the stiffer substrate, it becomes the leading edge. Further, the moving individual clearly accelerates as soon as it crosses the boundary between the two matrix regions (3.6 μm/s versus 4.5 μm/s, Fig. 5c), as experimentally observed in [8] for fibroblasts crawling over polyacrylamide sheets. An increment of the adhesive area is observed as well when the cell shifts over the stiff region.

In the case (b), the external potential forces the cell to move toward the north-east corner of the domain (see Movie 2 and Fig. 5b). However, as soon as the individual approaches the soft region, it changes orientation, and starts moving and elongating parallel to the boundary between the two substrate regions. These outcomes may be compared to the experimental observations obtained by Lo et al. in [46], who cultured fibroblasts on the already described substrate system, i.e., characterized by two areas with different Young's modulus. In particular, Lo and colleagues seeded cells at low density to minimize the effects of intercellular interactions and to avoid that pulling or pushing forces from neighbors individuals may alter cell substrate probing processes (thereby

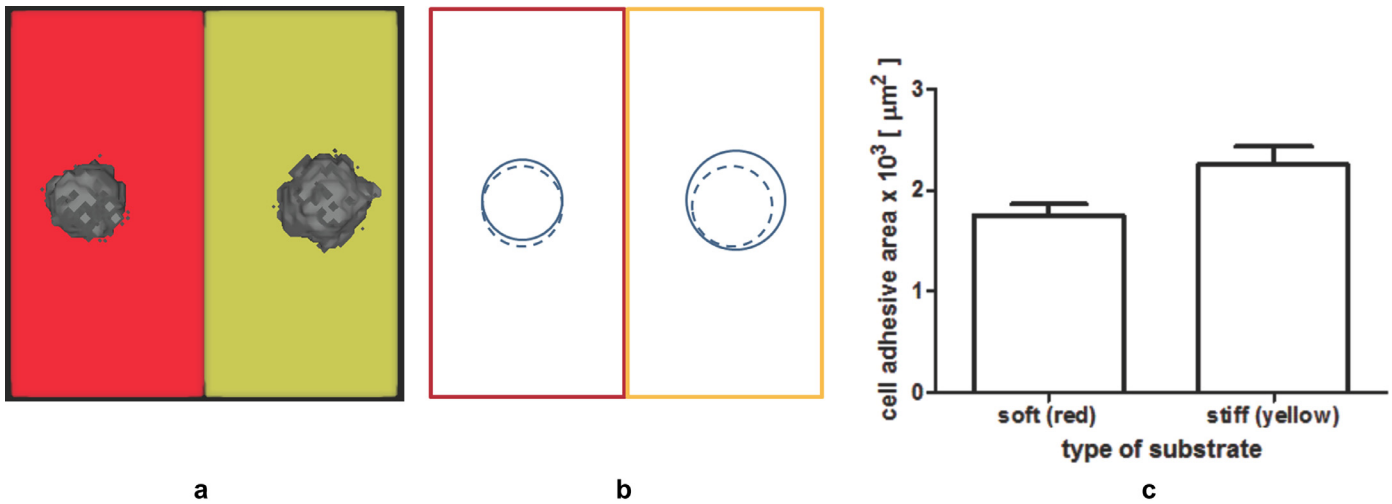

Fig. 4. Two cells are initially seeded on a soft (red) and a stiff (yellow) substrate, respectively. (a) Simulation snapshot of the final positions (i.e., at MCS = 500 corresponding to nearly 16 min) of the two cells. (b) Initial (dashed) and final (plain) contour shapes give an idea of the position and the morphology of the two cells. (c) Cell adhesive area as a function of the type of substrate. The area is about 30% higher in the case of the cell seeded over the stiff substrate, due to the specific constitutive law given to cell rigidity (i.e., Eq. (6)). (For interpretation of the references to colour in this figure legend, the reader is referred to the web version of this article.)

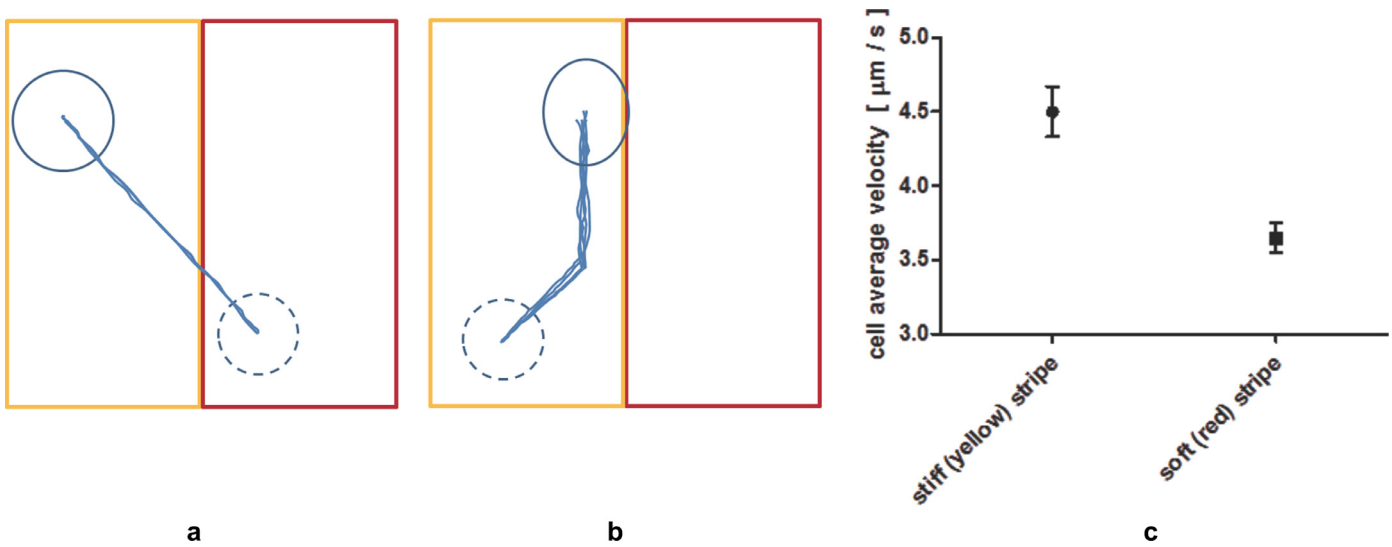

Fig. 5. Simulation for a substrate with soft (red) and stiff (yellow) subdomains. The trajectories of the cell center of mass as well as the initial (dashed) and the final (plain) cell contours are traced respectively for (a) a cell initially seeded at the south-east corner and an external potential introduced toward the north-west corner and (b) a cell initially seeded at the south-west corner and an external potential directed toward the north-east corner. (c) Cell average velocity over either the stiff and soft substrate. (For interpretation of the references to colour in this figure legend, the reader is referred to the web version of this article.)

impeding cells to freely move across the soft and the stiff regions). Then, cell migration was recorded over a time span of 10 h. Similarly to our numerical outcomes, the authors found that as cells move toward a stiffer substrate, new lamellipodia are formed in the direction of migration, thereby resulting in the dominant front end of the individuals. On the opposite, local retractions occur when cells approach a soft region, inducing therefore a change of direction. In a second series of experiments, Lo and co-workers showed that mechanical inputs triggered by substrate deformations might also control formation and retraction of lamellipodia. In particular, they externally pulled or pushed the substrate away or toward the cells center to find that, due to the centripetal forces exerted by the 3T3 fibroblasts on the substrate [46], in the first case less motion is produced, since cells experience a softening of the substrate, whereas in the second case the overall motion is increased, since cells perceive the substrate as stiffer. In the CPM model proposed here, the matrix substrates are not deformable, therefore the numerical simulations are unable to capture the experimental observations coming from this second set of assays.

3.3. Two stiff stripes embedded in a soft substrate

The third configuration that has been tested includes a soft substrate (again $\tau = S_1$ with $J_{C,S_1} = J_{soft} = 25 \times 10^{-15}$ kg/s^2) with two embedded stiff stripes (again $\tau = S_2$ with $J_{C,S_2} = J_{stiff} = 1 \times 10^{-15}$ kg/s^2), which are both 28 μm-wide (Fig. 2b). A cell Σ_1 is initially seeded at the south-west corner, whose rigidity is allowed to decrease following the constitutive law (Eq. (6)). An external potential is then introduced toward the north-east corner of the domain: its intensity $|\boldsymbol{v}_{ext}|$ is allowed to vary from a minimal value of 7×10^{-21} kg m/s^2 to a maximal value of 28×10^{-21} kg m/s^2. All simulations last 10,000 MCS, which correspond to nearly 5.5 h. In the case of a low $|\boldsymbol{v}_{ext}| = 7 \times 10^{-21}$ kg m/s^2 (see Fig. 6a and Movie 3), the cell typically migrates toward the first stiff substrate stripe:

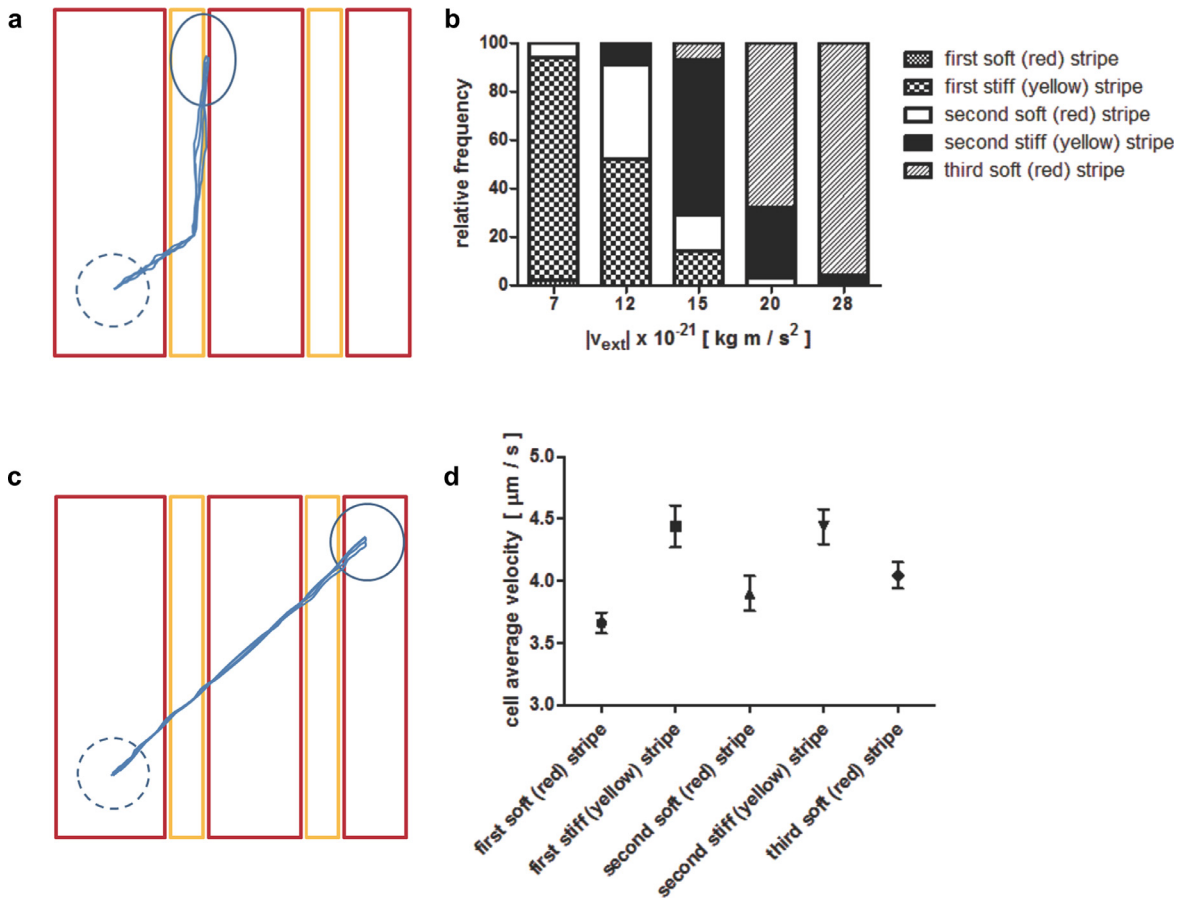

Fig. 6. Configuration with a soft (red) substrate with two embedded stiff stripes (yellow). (a) and (c) Simulations with $|\boldsymbol{v}_{ext}| = 7 \times 10^{-21}$ kg m/s^2 and $|\boldsymbol{v}_{ext}| = 28 \times 10^{-21}$ kg m/s^2 respectively. Representative cell trajectories are plotted together with the initial (dashed) and the final (plain) cell contours. (b) Relative cell frequency as function of $|\boldsymbol{v}_{ext}|$. (d) Cell average velocity over the different substrate regions in the case of $|\boldsymbol{v}_{ext}| = 28 \times 10^{-21}$ kg m/s^2. (For interpretation of the references to colour in this figure legend, the reader is referred to the web version of this article.)

then it remains stuck over it and goes on migrating along such a matrix region. Furthermore, its morphology, due to the dependency of its elasticity on the underneath type of substrate, changes as the crawling individual acquires an elongated shape. Such a behavior is due to the fact that the external potential is too low to overcome the adhesive interactions between the cell and the stiffest substrate: in particular, the individual has not energetic benefits (deriving from the external bias) to move further in the domain, i.e., to pass the first stiff stipe. The outcomes of our CPM are consistent to that observed for cells (i.e., endothelial cells or fibrosarcoma cells) seeded on 2D substrates (i.e., maleic acid copolymer surfaces) structured with fibronectin stripes which orient their actin fibers along the stripe direction [47–49].

On the other hand, if the modulus of the external potential increases, we have a higher percentage of cells that are able to cross the entire domain (Fig. 6b). In particular, when $|\boldsymbol{v}_{ext}|$ is maximal (i.e., 28×10^{-21} kg m/s^2, Fig. 6c and Movie 4), the cells constantly migrate at the north-east corner of the domain passing also the second stiff stripe. In this case, the cell average velocity increases over the stiff stripes (about 4.4 µm/s) whereas it varies between 3.6 µm/s and 3.9 µm/s over the soft regions (Fig. 6d). With the maximal external potential, cell morphology does not significantly vary, as the moving individuals typically maintain an almost hemispheric shape, without substantial elongation or increments in the adhesive area during the entire motion. They in fact behave as translating rigid bodies, subjected to an external high force. This interesting behavior is the consequence of the fact that the cells do not need to reorganize (nor have enough time to do it) to be able to crawl, as their motion is mainly due to the external bias: the specific substrate regions are only able to further accelerate (or partially slow down) cell movement, as previously commented. The numerical outcomes in the case of low or intermediate values of $|\boldsymbol{v}_{ext}|$ can be compared to those experimentally tested by Choi et al. [50] and Vincent et al. [51], where different cell phenotypes were seeded on micropatterned hydrogels with stiffness gradient. Although no external bias was introduced in such experimental configurations, a similar behavior may be observed. In the former work [50], the authors proposed two mechanically-patterned hydrogels: one constituted by 100 µm stiff (10 kPa) and 500 µm soft (1 kPa) stripes and one containing 500 µm stiff (10 kPa) and 100 µm soft (1 kPa). First, Adipose-derived Stem Cells (ASCs) and C2C12 myoblasts were allowed to adhere and both were able to sense the stiffness gradient and to migrate toward the stiffer stripes (i.e., durotaxis) [46]. Such behavior was also observed when cells were far away from the stripe interface (around 250 µm). Nevertheless, since cells only detect stiffness differences over short distances (around some microns) [52], in this case the authors implied that the phenomenon was mostly due to random walk toward the interface rather than to durotaxis itself. Regarding the morphology of the cells, both ASCS and C2C12 myoblasts aligned in the direction of the long axis of the stripe as we observe in our numerical simulations (Fig. 5a and Movie 3) in the case of low intensity of the external potential. Second, less contractile cells such as neurons were seeded on the hydrogels, which did not show any preferential adhesion confirming previous experimental observations according to which they prefer a softer niche [53].

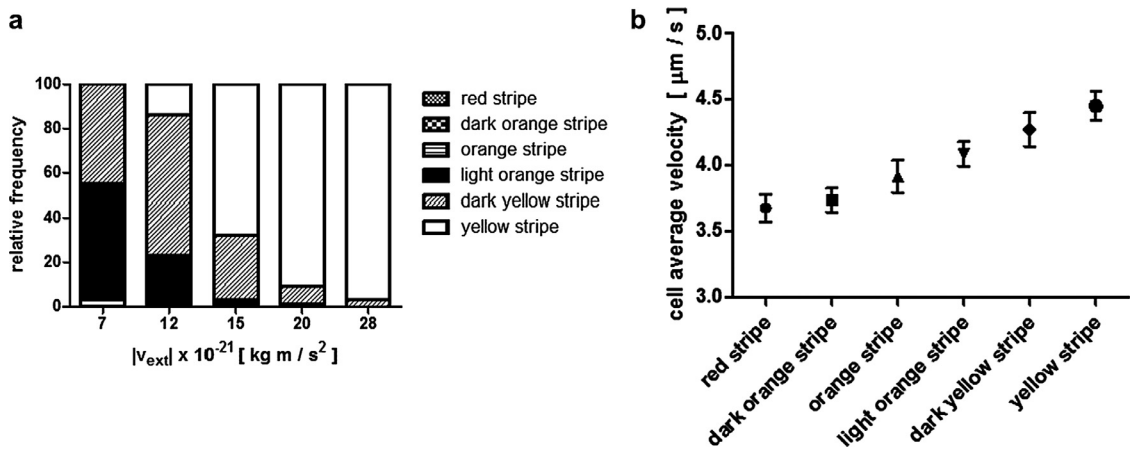

Fig. 7. Results for the simulation with a soft to stiff gradient (Section 3.4). (a) Relative cell frequency as $|\boldsymbol{v}_{ext}|$ increases. (b) Average cell velocity over the different substrate regions in case of $|\boldsymbol{v}_{ext}| = 28 \times 10^{-21}$ kg m/s^2.

In the latter work [51], the authors developed three types of polyacrylamide (PA) hydrogel systems of stiffness gradients: physiological (1 Pa/µm), pathological (10 Pa/µm) and step (100 Pa/µm). The step stiffness gradient, which is the configuration of interest for the simulations presented above in this section, was constituted by 500 µm wide regions of soft PA alternated with ~100 µm wide stripes of stiff hydrogel producing a stripped stiffness profile. MSCs were plated and they spread and attached independently of the gradient strength or the stiffness within hours after the seeding, whereas after 3 days they started to migrate toward stiffer regions. Additionally, cells crawled at 18 ± 0.7 µm/h, which is approximately sixfold faster than on the other gradient configurations discussed in the same paper (i.e. physiological and pathological) and confirms that durotaxis velocity is influenced by gradient strength [11].

3.4. Stiffness gradient

In this section, we present the results for a simulation involving a substrate made of six successive stripes (i.e., $\tau = S_i$ where $i = 1, \ldots, 6$, each 46 µm-wide) which are organized to obtain a soft-to-stiff gradient from the left to the right side of the domain (from the red to the yellow subdomains). Such substrate regions are characterized by different cell adhesive affinity, i.e., J_{C,S_i}, which vary from $J_{C,S_1} = J_{soft} = 25 \times 10^{-15}$ kg/s^2 to $J_{C,S_6} = J_{stiff} = 1 \times 10^{-15}$ kg/s^2, respectively (see Fig. 2c and the corresponding caption for the specific details). A cell Σ_1 is initially seeded at the south-west corner and an external potential is introduced toward the north-east corner of the domain, whose magnitude $|\boldsymbol{v}_{ext}|$ is varied again from a minimal value of 7×10^{-21} kg m/s^2 (Movie 5) to a maximal value of 28×10^{-21} kg m/s^2 (Movie 6). The rigidity ν_{Σ_1} of Σ_1 is allowed to decrease (from the usual initial high value of $\nu_C = 25 \times 10^{-3}$ kg/s^2 m^2) with a law analogous with Eq. (6), but which takes into account of the presence of different types of substrates, i.e.,

$$\nu_{\Sigma_1}(t) = \begin{cases} \max(\nu_{\Sigma_1}(t-1) - \nu_i; \nu_t) \\ \quad \text{if } \exists(\boldsymbol{x}, \boldsymbol{x}' \in \Omega'_{\boldsymbol{x}}) : \boldsymbol{x} \in \Sigma_1 \text{ and } \boldsymbol{x}' \in S_i; \\ \nu_{\Sigma_1}(t-1) \qquad \text{else,} \end{cases} \tag{8}$$

where t is the actual MCS, ν_t is the usual threshold value (equal to 10^{-2} kg/s^2 m^2) and $i = 2, \ldots, 6$. In this respect, $\nu_i = 0.05 \times 10^{-3}$, 0.06×10^{-3}, 0.1×10^{-3}, 0.2×10^{-3}, 1×10^{-3} kg/s^2 m^2 while the cell is in contact with substrate S_2, S_3, S_4, S_5, S_6, respectively. ν_{Σ_1} remains indeed constant and equal to ν_C if the cell is located over the softest substrate S_1. All the resulting simulations last 10,000 MCS (5.5 h). As reproduced in Fig. 7a, the percentage of cells able to reach the north-east corner increases concomitantly with increments of $|\boldsymbol{v}_{ext}|$. Moreover, by fixing $|\boldsymbol{v}_{ext}| = 28 \times 10^{-21}$ kg m/s^2, it is possible to observe that the cell average velocity increases from 3.6 µm/s to 4.4 µm/s as they move from softer to stiffer substrates (Fig. 7b). This result is coherent with the model outcomes of the previous set of simulations (i.e., see Fig. 6c and d), where we have observed that in the case of very high external potential cells accelerate while crossing on stiffer matrix regions, even if they do not significantly undergo morphological transitions.

A similar configuration was experimentally proposed by Cheung et al. [10] who, using a microfluidics-based lithography technique, fabricated a micropatterned cell-adhesive substrate made of a series of PEG-fibrinogen hydrogels with uniform stiffness ranging from 0.7 to 50 kPa. Human Foreskin Fibroblasts (HFFs) were then plated and their migratory trajectories were analyzed over 22 h. The authors found that the cells that were initially seeded on a stiffness frontier tended to migrate toward the stiffer region, while cells plated on uniform stiffness spread in both directions.

3.5. Role of the characteristic dimension of the gradient stiffness

The external potential introduced in most of the previous sets of simulations, is an artificial term that is included in the Hamiltonian to bias and sustain cell movement across the entire matrix substrate. In experimental assays, the directional component in cell motion is typically established by geometrical cues, such as microtracks and microchannels [54,55], or gradients of soluble or insoluble chemical substances (chemotaxis and haptotaxis, respectively) or, in the case of our interest, gradients of substrate stiffness [10,51]. However, we have observed from our simulations that the sequence of different types of substrate stripes employed in the previous section does not suffice to determine a persistent cell movement across the entire matrix, since a high enough external potential has to be included to allow cells reach the north-east corner of the domain (see the plot in Fig. 7a). The reason of this discrepancy between computational and experimental outcomes relies in the fact that "real cells", once established a direction of movement, are able to dramatically orient their cytoskeleton (via the polarization of actin filaments) and, eventually, start a persistent shape-dependent locomotion. This way, real individuals are able to cross also large portions of substrates without slowing down or changing direction. Such a cell behavior cannot be captured in our approach since we do not include a proper model component reproducing selected intracellular cytoskeletal dynamics (in this respect, the interested reader may refer to [56,57],

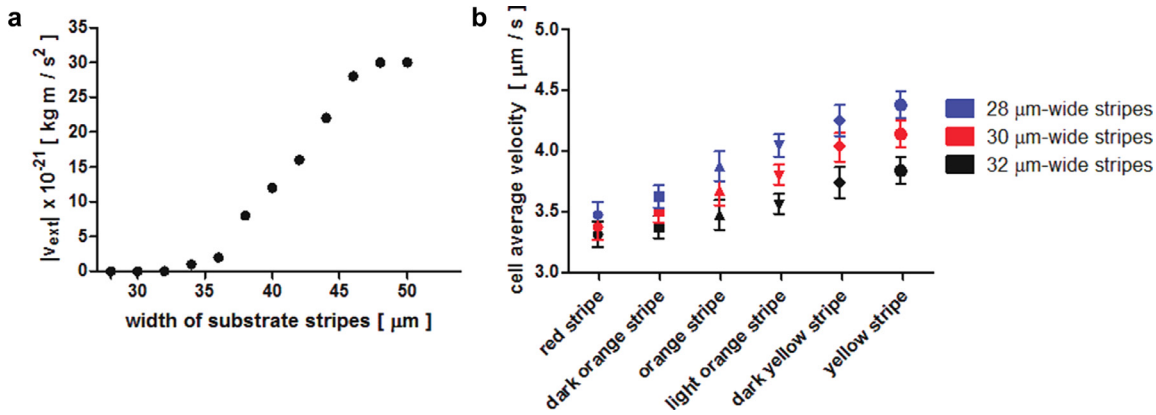

Fig. 8. Results for the simulations with a soft to stiff gradient (Section 3.5). (a) $|\boldsymbol{v}_{ext}|$ necessary to allow cells reach the opposite border of the domain versus width of substrate stripes. (b) Average cell velocity over the different substrate regions for different widths of the matrix stripes in case of a stiffness gradient sufficient fine-grained to have a cell persistent movement even in the absence of an external potential.

where polarization processes and the subsequent cell persistent movements are simulated in CPMs either by introducing an asymmetric correction to the Boltzmann probability law or by adding a further inertial term in the Hamiltonian). The CPM cells of our model are only able to isotropically spread (due to decrements in their rigidity upon contact with stiff substrates) or elongate following the geometry of the underlying matrix region in order to maximize their adhesive interactions with the stiffer areas of the domain (but only when the external potential is substantially low, see Fig. 6a and c). However, the model presented in this paper can be used to predict if a sustained cell motion can be achieved by only varying the geometrical characteristics of the matrix substrate. With this purpose in mind, we employ the same type of domain as in Section 3.4, but we progressively decrease the width of the substrate stripes. We then evaluate the minimal magnitude of the external potential needed by cells to reach the border of the domain opposite to their initial position (again the south-west corner). Cell rigidity follows the law in Eq. (8) and the simulations last 10,000 MCS (5.5 h). As summarized in panel (a) of Fig. 8, we can observe a tri-phasic behavior. For sufficiently wide stripes (i.e., $> 45\,\mu$m), a cell sustained movement results only with very high external potentials (i.e., $>25\ \times 10^{-21}$ kg m/s^2). Then, for lower stripe widths (i.e., in the range of 35–45 μm) the critical value of the external potential modulus decreases almost linearly. Finally, for low enough stripe widths (i.e., $<35\,\mu$m), the potential necessary to have a sustained cell movement significantly drops, until becoming negligible for stripe widths lower than 35 μm (Movie 7). Summing up, we can state that the characteristic dimension of the stiffness gradient (here determined by the width of the matrix stripes), which allows a persistent cell movement without the artificial help of an external bias, is lower than the mean cell diameter (i.e., that in our simulations is around 40–45 μm). From a computational viewpoint, the rationale of this behavior is that when a CPM cell is located on a given substrate stripe it is however able to wandering its close proximity (due to the stochastic Metropolis algorithm) which, if the stripe width is low enough, includes the neighboring matrix region. In this respect, the CPM cell simultaneously experiences the adhesive affinity with a couple of neighboring substrate stripes and then it moves toward the stiffer one, thereby advancing across the domain. Such a process is reiterated for all pairs of substrate stripes, thereby resulting in a sustained directional movement. These results can be interpreted from an experimental viewpoint as a prediction on the fact that cells may exhibit a persistent motion also without an intracellular polarization, i.e., by only maintain an amoeboid movement, if the substrate stiffness gradient is sufficiently fine-grained.

We finally conclude this section by analyzing how cell velocity is affected by the wide of the substrate stripes, in the range of values sufficiently low to have a sustained cell crawling in the absence of an external potential (i.e., $<35\,\mu$m). As it is possible to see in panel (b) of Fig. 8, lower widths of the substrate regions (which means, as previously seen, more fine-grained stiffness gradients) results in increments in cell average velocity. From the computational viewpoint, this is due to the fact that the more the different stripes of the matrix are small, the more the previously described cell probing mechanism is facilitated and accelerated, thereby resulting in higher cell average velocities.

3.6. Soft squares embedded in a stiff substrate

As a final simulation, we test the substrate configuration in Fig. 2d, where four soft squares ($\tau = S_1$ with $J_{C,S_1} = J_{soft} = 25 \times 10^{-15}$ kg/s^2) are embedded in a stiff substrate ($\tau = S_2$ with $J_{C,S_2} = J_{stiff} = 1 \times 10^{-15}$ kg/s^2) at its three corners (north-west, north-east and south-east) and at the center. A cell Σ_1 is initially seeded at the south-west corner and an external potential is introduced toward the north-east corner of the domain, whose magnitude $|\boldsymbol{v}_{ext}|$ has been set equal to an intermediate 14×10^{-21} kg m/s^2. As usual, cell rigidity is allowed to decrease according to Eq. (6) and the observation time is 10,000 MCS (i.e., nearly 5.5 h). The cell starts moving in the direction determined by the potential with a trajectory of approximately 45° but, as soon as it encounters the central soft square, the cell avoids and circumvents it. As the original path is recovered, the cell needs to squeeze between the north-east square and the substrate frontier in order to achieve the target corner of the domain (Movie 8 and Fig. 9). The choice of the migration track may depend on the initial position of the cell. In the present simulation, the cell is seeded along the substrate diagonal, thus the probability of circumventing the central soft square counter clockwise (as it happens here) or clockwise are the same. However, if the cell is seeded slightly downward and/or right, it will most certainly employ a counter clockwise trajectory, whereas if it is plated upward, it will probably follow a clockwise path. It is useful to notice that with a significantly higher modulus of the external potential the cell would have been able to pass across the soft regions, without deforming to avoid them, coherently with the simulations proposed in Fig. 6c.

This configuration is similar to that proposed in [23] where the cell must avoids two slipping regions in order to reach the external cue placed at 45°. Although the employed numerical approaches are substantially different, taken together the outcomes confirm

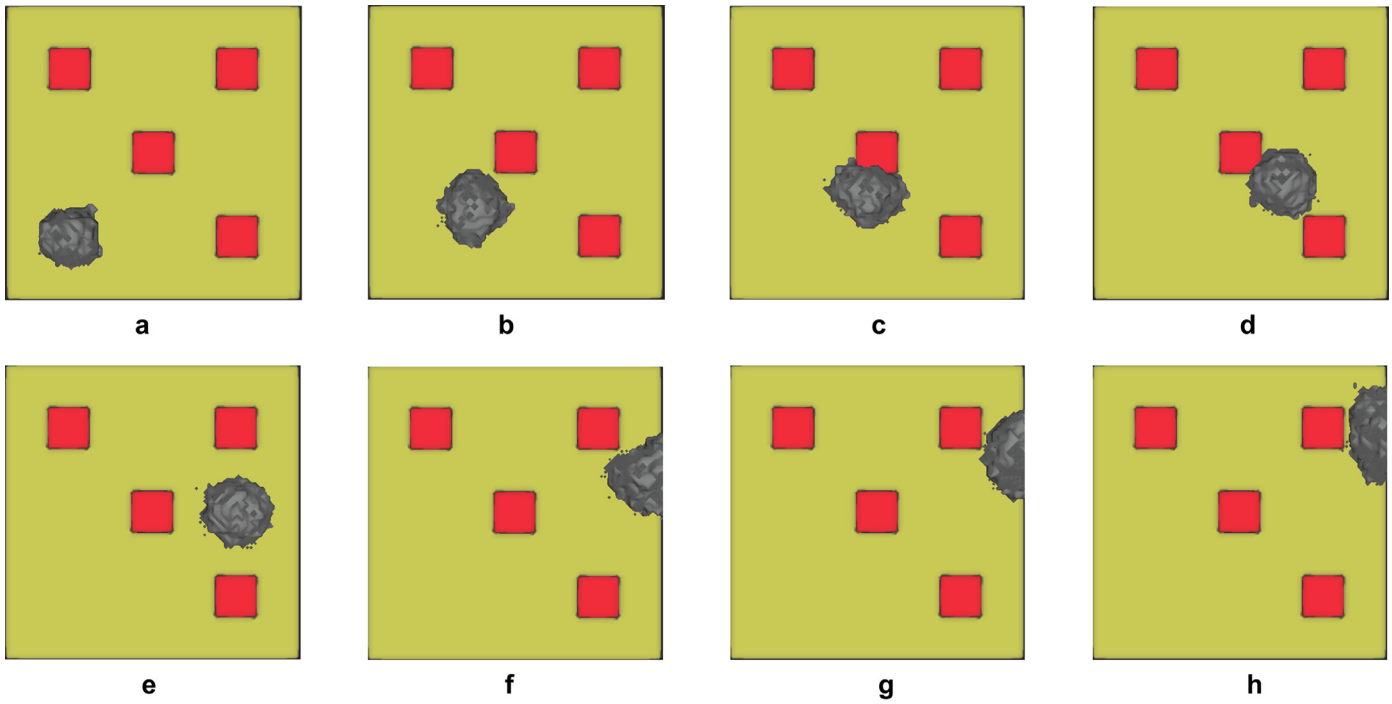

Fig. 9. Snapshots from a representative simulation dealing with a domain with four soft squares (red) embedded in a stiff substrate (yellow). The cell is initially seeded at the south-west corner and migrates in the direction of an external potential ($|\boldsymbol{v}_{ext}| = 14 \times 10^{-21}$ kg m/s^2), i.e., toward the north-east corner. Snapshots are taken at 2 min (a), 30 min (b), 1.5 h (c), 2 h (d), 2.5 h (e), 3.5 h (f), 4.5 h (g) and 5.5 h (g). (For interpretation of the references to colour in this figure legend, the reader is referred to the web version of this article.)

the tendency of the cell to migrate over stiffer substrates where the higher adhesion forces may be developed.

4. Conclusions

In this paper we have proposed a three-dimensional CPM approach to simulate single cell migration over matrix domains in which soft and stiff regions are combined.

The CPM method is becoming an increasingly common technique for the mathematical modeling of a wide range of biological phenomena, including avascular and vascular tumor growth [58–61], gastrulation [62], skin pigmentation [63], yeast colony growth [64], stem cell differentiation [65], fruiting body formation of *Dictyostelium discoideum* [66], epidermal formation [67], hydra regeneration [66], retinal patterning [68], wound healing [69,70], biofilms [71], chick limb-bud growth [72–74], cellular differentiation and growth of tissues, blood flow and thrombus development [75–77], angiogenesis [70,78–81], dynamics of vascular cells [82–85], cell scattering [86], cell migration on and within matrix environments [56,57,87]. Notably, in [88] the authors introduced a compartmentalized approach to subdivide a *Myxococcus xanthus* into strings of subcellular domains with different rigidity, this in order to give the bacterium a particular geometry and to control its overall length. Further, in [89] a keratocyte has been represented with a set of undifferentiated hexagonal subunits, which has allowed to reproduce its polarization during motion. In this respect, it is useful to underline that, as commented in [25], although these approaches are correct, the fact that the proposed subcellular compartments do not have an immediate or direct correspondence with real subcellular elements, has limited the practicality and the usefulness of the relative models. The most accurate way of realistically reproducing different and extremely complex cell morphologies is to compartmentalize them according to the compartmentalization “suggested in nature”, and thus to explicitly represent for instance the plasmamembrane (PM), the cytosolic region, the nucleus, and other intracellular organelles (e.g., mitochondria, ribosomes, Golgi apparatus, and secretory granules). This way is in fact possible, for example, to localize within the proper cell compartment selected biochemical pathways and/or to study the role play by the nucleus in cell movement, given its higher rigidity with respect to the surrounding cytoplasm [56,57,87].

Key benefits of the CPM energetic formalism are its simplicity and extensibility: almost any biological mechanism can in fact be included in the model, simply by adding an appropriate generalized potential term in the Hamiltonian functional. For instance, it is possible to easily comprehend the importance of each mechanism involved in the simulated phenomenon by only altering the relative Potts parameter, so that the other terms in the Hamiltonian scale accordingly. In particular, by equating all the other terms to zero, it is possible to understand whether a mechanism is individually capable of producing the phenomenon of interest or whether it requires cooperative processes. Further critical features of the CPM (compared to alternative cell-based modeling approaches that represent biological individuals as point particles, such as Interacting Particle Systems or purely discrete models, or fixed-sized spheres or ellipsoids, such as Cellular Automata) is that i) it differentiates between bound and unbound regions of cell membranes and ii) morphological changes can be easily and realistically reproduced. These characteristics have been fundamental in our choice of using a CPM to describe the phenomenon of our interest since they are particularly suitable to implement our two main model assumptions, drawn according to the experimental observations reported in the literature: i) the adhesiveness of cells changes according to the substrate stiffness, that models the fact that higher traction forces and more stable focal points are generated over a stiffer substrate [16,35–38] and ii) each cell adapts its morphology as a function of the substrate stiffness so that over a soft region it maintains a rounded shape, whereas over a stiffer domain a significant spreading occurs [39–43]. The considerations above are in remarkable agreement with the scholarly dissertation proposed by

Voss-Böhme in the conclusive section of her article [33]. She in fact argued that the application of CPMs is reasonable when the biological problem of interest involves "considerable variability in cell sizes and shapes", which is the case of the cell morphological transitions due to contact with soft/stiff substrates. On the opposite, when "essentially isotropic, non-polarized cells of uniform size are considered", it would be preferable the use of more coarse-grained modeling approaches, like the already cited Cellular Automata or Interacting Particle Systems, which are better analyzed both mechanistically and analytically.

Further, we have opted for a 3D setting since the adhesive interactions between cells and matrix substrates occur *under* the cell body (i.e., they are localized over the contact area between the cells themselves and the underneath substrate). In bi-dimensional CPMs cell–matrix interactions instead occur only "laterally", as the cells do not move *on* substrates but *within* the same plane as the matrix. Indeed, a three-dimensional domain is more appropriate to reproduce an adhesive-driven cell migration.

We have then used our CPM-based approach to test cell behavior in different domain configurations, where soft and stiff substrates coexisted. In particular, the numerical outcomes have been consistently compared to specific experimental data, in terms of cell morphology, distance covered, spreading/adhesive area and migration speed. In this respect, following the dichotomy proposed in the already cited work by Voss-Böhme [33], we have interpreted our CPM as a *phenomenological* method. In particular, the resulting remarkable agreement (not only qualitative but also quantitative) between in vitro and in silico data has allowed us to conclude that our approach, although strongly simplified, was able to capture the main mechanisms underlying cell migration in presence of durotaxis. We have finally turned to use our model in a *predictive* manner, with the aim to analyze how the external potential and the critical dimensions of a substrate stiffness gradient (here represented by the width of the different types of matrix stripes) affect cell movement. In this respect, we have found that cells are able to achieve a sustained cell migration in the absence of an external bias (and in the absence of intracellular polarization mechanisms) where the underneath matrix is characterized by a sufficient fine-grained gradient of rigidity.

However, our approach is not free of some serious shortcomings. First, it does not reproduce the active and continuous reorganization of the cytoskeleton, which provides the support for cells and mediates their coordinated and directed movements, mainly in response to mechanical tensions and stresses exchanged with the underneath substrate. In this respect, selected geometrical and mechanical properties of the cells, such their elongation and elasticity, should evolve according to a model of actin filament dynamics, which are powered, for example, by ATP (adenosine triphosphate) hydrolysis and controlled by inside-out signaling mechanisms transmitted from and by the extracellular matrix via focal adhesion points. Further, in our model, the substrates are not deformable and therefore it has not been possible to account how the matrix reacts to the probing processes exerted by crawling cells. Finally, it is useful to underline that our specific CPM application does not suffer of the limitation that Voss-Böhme proved to characterize most CPMs (see again [33]), i.e., cells die out in the long-run due to modifications in the original Metropolis algorithm. We have in fact focused on relatively short observation times: our model has indeed worked in a well-behaved parameter regime where the temporal evolution of the simulated system has been still directed toward the minimization of the Hamiltonian functional and the non-controlled, voter-like part of the lattice updates has been negligible.

Movie 1 Simulation of cell migration over a stiff-soft substrate (yellow = stiff region, red = soft region) in presence of an external potential directed toward the north-west corner (Section 3.2). The cell is initially seeded at the south-east corner.

Acknowledgments

This work was initiated and partially completed while Rachele Allena was a visitor to the Dipartimento di Scienze Matematiche of the Politecnico di Torino funded by the Gruppo Nazionale per la Fisica Matematica (GNFM).

Appendix

A.1. Morphological and migratory determinants

The *position* of a cell was established by the coordinate of its center of mass (CM). In particular, a cell was assumed to be located on a given type of substrate if its center of mass was located on that matrix region. In this respect, the migratory *trajectory* of a cell was generated by tracking the position of its center of mass at each time step (i.e., at each MCS).

The *adhesive area* of a cell was defined as the extension of its surface in contact with the substrate of interest at the final observation time.

The *average velocity* of an individual on a given type of substrate was measured as the ratio between the width of the substrate region itself (which is clarified for each simulation setting) and the time needed by the cell to cross it. In this respect, to obtain the amount of time spent by a cell to pass a given matrix region it is sufficient to multiply the corresponding average velocity for the width of the substrate of interest.

A.2. Statistics

In the plots, we represented cell trajectories coming from 10 independent and randomly chosen simulations. A number of 10 was chosen since we observed that it was sufficient to have a correct interpretation of the simulation outcomes but it was also low enough to have an acceptable graphical quality, as too many cell paths overlapped one to each other, thereby resulting undistinguishable.

Cell average velocity and adhesive area were instead given in the corresponding graphs as mean $\pm$ sd over 100 independent simulations.

In the plots representing the cell final distribution on the different types of substrate, the relative frequency was given by the number of individuals that, over 100 independent simulations, were located over each matrix region at the end of the observation time. Indeed, the sum of the relative frequencies is, in all cases, equal to 100.

Finally, dashed and plain ellipsoids representing, respectively, initial and final cell morphologies in a given simulation setting were established by interpolating the cell adhesive areas coming from 10 independent simulations (typically the ones used to track the cell trajectories for the same simulation setting). Obviously, the initial cell position was the constant for each simulation setting, whereas the initial cell shape was the same for all cases (i.e., a hemisphere of 20 μm of radius).

A.3. Parameter estimates

Given the energetic nature of the CPM, a direct one-to-one correspondence between model parameters and experimental quantities is not straightforward (as commented also in [27] and in [90]). In particular, as explained in details in [33], the CPM parameters can be subdivided in i) directly interpretable and measurable

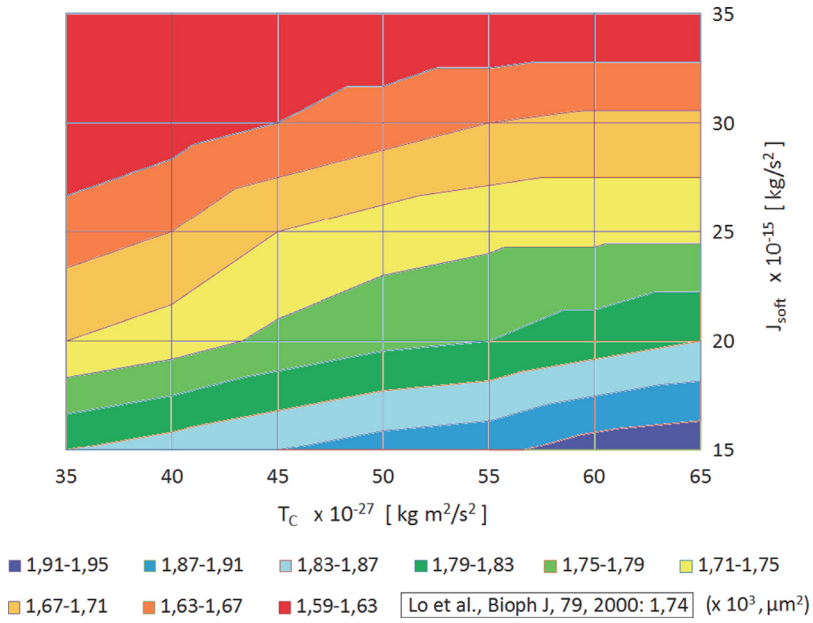

Fig. 10. Cell adhesive area at 5.5 h, obtained from CPM simulations for different values both of the Boltzmann temperature T_C and of the adhesiveness between the cell and the softest substrate, i.e., J_{soft}. Values are given as the mean over 100 simulations. The experimental value measured by Lo and co-workers in corresponding conditions is 1.74 $\times$ 10^3 μm^2. From this plot, it was indeed possible to observe that the parameter region pseudo-colored in yellow gave the best fitting couples of coefficients. In particular, we opted for $T_C = 50 \times 10^{-27}$ kg m^2/s^2 and $J_{soft} = 25 \times 10^{-15}$ kg/s^2. (For interpretation of the references to colour in this figure legend, the reader is referred to the web version of this article.)

quantities, such as cell geometrical dimensions ii) effective parameters that subsume various cellular and subcellular properties, such as the adhesive strength and the elastic moduli determining cell geometrical attributes iii) "merely technical coefficients", such as the Boltzmann temperature, that has been interpreted in different ways by CPM authors (in this work, we opted to link the value of T_C to an intrinsic cell motility, i.e., the amplitude of cell boundary fluctuations: consistently, we therefore added the subscript "C" to the coefficient T_C). However, a plausible parameter setting was inferred by a proper comparison with experimental findings, taking also advantage of selected sensitivity analysis performed in other CPM-based works. First, the initial/target dimensions of our virtual cells were consistent with the measures of NIH 3T3 mouse fibroblasts used by Lo and colleagues [8] for their assays on durotaxis. Since, as previously seen, we did not include in our model any nutrients and therefore cells were not allowed to grow during migration, we set a high $\kappa_C = 25 \times 10^{-9}$ kg/(s^2 m^4) to keep cell volume fluctuations within a few per cent. Such a specific value was taken from other CPMs dealing both with single cell dynamics [82] and with multicellular phenomena [91], where it was estimated after some trials. Further, observing from the data by Lo et al. [46] that 3T3 cells seeded on soft enough substrates did not significantly spread or undergo morphological transitions, we set a high value $\nu_C = 25 \times 10^{-3}$ kg/(s^2 m^2) also for the intrinsic cell rigidity which, as previously seen, can decreases (in our work) only upon cell contact with stiffer substrates. This choice is consistent with other CPM-based approaches [57,70,82,91] that employed similar values (i.e., $\geq$ 15) to model an initially low cell deformability.

We then turned to estimate both the Boltzmann temperature T_C and the cell-substrate adhesiveness, denoted as J_{soft} thoughout the paper, in the case of the softest matrix regions considered in this paper (i.e., the ones pseudo-colored in red in the simulations, typically identified by $\tau = S_1$). In particular, we looked for the couple of coefficients (T_C, J_{soft}) that simultaneously best fitted the in vitro results by Lo and co-workers in the corresponding experimental setting (i.e., collagen-coated polyacrylamide substrate properly manipulated to obtain a low Young's modulus of 14 kPa) in terms of cell adhesive area (which was called by Lo and colleagues "projected area" [46]). As it is possible to observe in Fig. 10, there is a quite large range of values that matched experimental and computational data (i.e., the yellow area of the graph): however, we opted for the intermediate couple of coefficients $T_C = 50 \times 10^{-27}$ kg m^2/s^2 and $J_{soft} = 25 \times 10^{-15}$ kg/s^2. Decrements in cell-substrate adhesive strength and in cell rigidity, allowed in our model as a consequence of cell contact with stiffer matrix regions, were then performed until selected threshold values, i.e., $\nu_t = 10^{-2}$ kg/s^2 m^2 and $J_{stiff} = 1 \times 0^{-15}$ kg/s^2, respectively. In particular, ν_t was the lowest value of cell rigidity that permitted to avoid unrealistic (often disconnected) cell shapes. J_{stiff}, i.e., the adhesive force between cells and the stiffest substrates (the ones pseudo-colored in yellow in the simulation snapshots, typically labeled by $\tau = S_2$, except from the case of the simulations dealing with the stiffness gradient) was instead the lowest value for which cells did not start to slow down during migration. In fact, as studied in details in [87], a too high cell-substrate adhesiveness partially inhibits cell movement, as CPM cells are not able to detach from the matrix component if the corresponding J-parameter is too low. Finally, the cell-medium contact strength was set equal to J_{soft} (i.e., $= 25 \times 10^{-15}$ kg/s^2). The rationale of this choice relied in the fact that for lower values of $J_{C,M}$ cells detached from the substrate and fluctuate in the middle of the medium, which was obviously an unrealistic situation. On the opposite, too high values of $J_{C,M}$ (i.e., $> 30 \times 10^{-15}$ kg/s^2) forced cells to completely lay down on the matrix, in order to minimize their contact surface with the medium, but also this situation was not plausible. Finally, the correspondence between 1 MCS and 2 s of actual time was taken from another CPM reproducing three-dimensional cell migration in matrix environments [87]. Further, we observed that this setting resulted in a remarkable accordance, in terms of cell velocity, between computational and experimental results: our CPM cells in fact move at speeds in a range of (3, 5) µm/s, which

is consistent with the values measured by Vincent and colleagues [51] in the case of MSCs plated on polyacrylamide (PA) hydrogels with selected stiffness.

Supplementary materials

Supplementary material associated with this article can be found, in the online version, at doi:10.1016/j.mbs.2016.02.011.

References

[1] R.L. Juliano, S. Haskill, Signal transduction from the extracellular matrix, J. Cell Biol. 120 (1993) 577–585.
[2] P. Martin, Wound healing–aiming for perfect skin regeneration, Science 276 (1997) 75–81.
[3] L.R. Bernstein, L.A. Liotta, Molecular mediators of interactions with extracellular matrix components in metastasis and angiogenesis, Curr. Opin. Oncol. 6 (1994) 106–113.
[4] D.A. Lauffenburger, A.F. Horwitz, Cell migration: a physically integrated molecular process, Cell 84 (1996) 359–369.
[5] H. Harris, Role of chemotaxis in inflammation, Physiol. Rev. 34 (1954) 529–562.
[6] K.R. Robinson, The responses of cells to electrical fields: a review, J. Cell Biol. 101 (1985) 2023–2027.
[7] S. Li, P. Butler, Y. Wang, Y. Hu, D.C. Han, S. Usami, et al., The role of the dynamics of focal adhesion kinase in the mechanotaxis of endothelial cells, Proc. Natl. Acad. Sci. USA 99 (2002) 3546–3551, doi:10.1073/pnas.052018099.
[8] C.M. Lo, H.B. Wang, M. Dembo, Y.L. Wang, Cell movement is guided by the rigidity of the substrate, Biophys. J. 79 (2000) 144–152, doi:10.1016/S0006-3495(00)76279-5.
[9] M. Raab, J. Swift, P.C.D.P. Dingal, P. Shah, J.-W. Shin, D.E. Discher, Crawling from soft to stiff matrix polarizes the cytoskeleton and phosphoregulates myosin-II heavy chain, J. Cell Biol. 199 (2012) 669–683, doi:10.1083/jcb.201205056.
[10] Y.K. Cheung, E.U. Azeloglu, D.A. Shiovitz, K.D. Costa, D. Seliktar, S.K. Sia, Microscale control of stiffness in a cell-adhesive substrate using microfluidics-based lithography, Angew. Chem. Int. Ed. 48 (2009) 7188–7192, doi:10.1002/anie.200900807.
[11] B.C. Isenberg, P.A. DiMilla, M. Walker, S. Kim, J.Y. Wong, Vascular smooth muscle cell durotaxis depends on substrate stiffness gradient strength, Biophys. J. 97 (2009) 1313–1322, doi:10.1016/j.bpj.2009.06.021.
[12] I.B. Bischofs, U.S. Schwarz, Cell organization in soft media due to active mechanosensing, Proc. Natl. Acad. Sci. USA 100 (2003) 9274–9279, doi:10.1073/pnas.1233544100.
[13] A. Saez, M. Ghibaudo, A. Buguin, P. Silberzan, B. Ladoux, Rigidity-driven growth and migration of epithelial cells on microstructured anisotropic substrates, Proc. Natl. Acad. Sci. USA 104 (2007) 8281–8286, doi:10.1073/pnas.0702259104.
[14] L. Trichet, J.L. Digabel, R.J. Hawkins, S.R.K. Vedula, M. Gupta, C. Ribrault, et al., Evidence of a large-scale mechanosensing mechanism for cellular adaptation to substrate stiffness, Proc. Natl. Acad. Sci. USA 109 (2012) 6933–6938, doi:10.1073/pnas.1117810109.
[15] M. Raab, J. Swift, P.C.D.P. Dingal, P. Shah, J.-W. Shin, D.E. Discher, Crawling from soft to stiff matrix polarizes the cytoskeleton and phosphoregulates myosin-II heavy chain, J. Cell Biol. 199 (2012) 669–683, doi:10.1083/jcb.201205056.
[16] C.A. Reinhart-King, M. Dembo, D.A. Hammer, The dynamics and mechanics of endothelial cell spreading, Biophys. J. 89 (2005) 676–689, doi:10.1529/biophysj.104.054320.
[17] P. Moreo, J.M. García-Aznar, M. Doblaré, Modeling mechanosensing and its effect on the migration and proliferation of adherent cells, Acta Biomater 4 (2008) 613–621, doi:10.1016/j.actbio.2007.10.014.
[18] B. Harland, S. Walcott, S.X. Sun, Adhesion dynamics and durotaxis in migrating cells, Phys. Biol. 8 (2011) 015011, doi:10.1088/1478-3975/8/1/015011.
[19] I.V. Dokukina, M.E. Gracheva, A model of fibroblast motility on substrates with different rigidities, Biophys J. 98 (2010) 2794–2803, doi:10.1016/j.bpj.2010.03.026.
[20] F. Stefanoni, M. Ventre, F. Mollica, P.A. Netti, A numerical model for durotaxis, J. Theor. Biol. 280 (2011) 150–158, doi:10.1016/j.jtbi.2011.04.001.
[21] S.A. Sandersius, T.J. Newman, Modeling cell rheology with the subcellular element model, Phys. Biol. 5 (2008) 015002, doi:10.1088/1478-3975/5/1/015002.
[22] C.W. Harvey, F. Morcos, C.R. Sweet, D. Kaiser, S. Chatterjee, X. Liu, et al., Study of elastic collisions of *Myxococcus xanthus* in swarms, Phys. Biol. 8 (2011) 026016, doi:10.1088/1478-3975/8/2/026016.
[23] R. Allena, D. Aubry, "Run-and-tumble" or "look-and-run"? A mechanical model to explore the behavior of a migrating amoeboid cell, J. Theor. Biol. 306 (2012) 15–31, doi:10.1016/j.jtbi.2012.03.041.
[24] Graner, Glazier, Simulation of biological cell sorting using a two-dimensional extended Potts model, Phys. Rev. Lett. 69 (1992) 2013–2016.
[25] M. Scianna, L. Preziosi, Multiscale developments of the Cellular Potts Model, Multiscale Model. Simul. 10 (2012) 342–382, doi:10.1137/100812951.
[26] A. Balter, R.M.H. Merks, N.J. Popławski, M. Swat, J.A. Glazier, D.A.R.A. Anderson, P.M.A.J. Chaplain, D.K.A. Rejniak, The Glazier–Graner–Hogeweg Model: extensions, future directions, and opportunities for further study, Single-Cell-Based Models in Biology and Medicine, Birkhäuser, Basel, 2007, pp. 151–167. http://link.springer.com/chapter/10.1007/978-3-7643-8123-3_7 (accessed 29.07.15).
[27] J.A. Glazier, A. Balter, N.J. Popławski, D.A.R.A. Anderson, P.M.A.J. Chaplain, D.K.A. Rejniak, Magnetization to morphogenesis: a brief history of the Glazier–Graner–Hogeweg Model, Single-Cell-Based Models in Biology and Medicine, Birkhäuser, Basel, 2007, pp. 79–106. http://link.springer.com/chapter/10.1007/978-3-7643-8123-3_4 (accessed 29.07.15).
[28] N.J. Savill, R.M.H. Merks, D.A.R.A. Anderson, P.M.A.J. Chaplain, D.K.A. Rejniak, The Cellular Potts Model in biomedicine, Single-Cell-Based Models in Biology and Medicine, Birkhäuser, Basel, 2007, pp. 137–150. http://link.springer.com/chapter/10.1007/978-3-7643-8123-3_6 (accessed 29.07.15).
[29] A. Szabó, R.M.H. Merks, Cellular Potts modeling of tumor growth, tumor invasion, and tumor evolution, Front. Oncol. 3 (2013) 87, doi:10.3389/fonc.2013.00087.
[30] E. Ising, Beitrag zur Theorie des Ferromagnetismus, Z. Phys. 31 (1925) 253–258, doi:10.1007/BF02980577.
[31] R.B. Potts, Some generalized order-disorder transformations, Math. Proc. Cambridge Philos. Soc. 48 (1952) 106–109, doi:10.1017/S0305004100027419.
[32] N. Metropolis, A.W. Rosenbluth, M.N. Rosenbluth, A.H. Teller, E. Teller, Equation of state calculations by fast computing machines, J. Chem. Phys. 21 (1953) 1087–1092, doi:10.1063/1.1699114.
[33] A. Voss-Böhme, Multi-scale modeling in morphogenesis: a critical analysis of the Cellular Potts Model, PLoS One 7 (2012) e42852, doi:10.1371/journal.pone.0042852.
[34] M.S. Steinberg, Reconstruction of tissues by dissociated cells. Some morphogenetic tissue movements and the sorting out of embryonic cells may have a common explanation, Science 141 (1963) 401–408.
[35] J.P. Califano, C.A. Reinhart-King, Substrate stiffness and cell area predict cellular traction stresses in single cells and cells in contact, Cell. Mol. Bioeng. 3 (2010) 68–75, doi:10.1007/s12195-010-0102-6.
[36] J.L. Tan, J. Tien, D.M. Pirone, D.S. Gray, K. Bhadriraju, C.S. Chen, Cells lying on a bed of microneedles: an approach to isolate mechanical force, Proc. Natl. Acad. Sci. USA 100 (2003) 1484–1489, doi:10.1073/pnas.0235407100.
[37] C.A. Reinhart-King, M. Dembo, D.A. Hammer, Endothelial cell traction forces on RGD-derivatized polyacrylamide substrata†, Langmuir 19 (2003) 1573–1579, doi:10.1021/la026142j.
[38] A.D. Rape, W.-H. Guo, Y.-L. Wang, The regulation of traction force in relation to cell shape and focal adhesions, Biomaterials 32 (2011) 2043–2051, doi:10.1016/j.biomaterials.2010.11.044.
[39] T. Yeung, P.C. Georges, L.A. Flanagan, B. Marg, M. Ortiz, M. Funaki, et al., Effects of substrate stiffness on cell morphology, cytoskeletal structure, and adhesion, Cell Motil. Cytoskeleton. 60 (2005) 24–34, doi:10.1002/cm.20041.
[40] M. Ghibaudo, A. Saez, L. Trichet, A. Xayaphoummine, J. Browaeys, P. Silberzan, et al., Traction forces and rigidity sensing regulate cell functions, Soft Matter 4 (2008) 1836, doi:10.1039/b804103b.
[41] A. Engler, L. Bacakova, C. Newman, A. Hategan, M. Griffin, D. Discher, Substrate compliance versus ligand density in cell on gel responses, Biophys. J. 86 (2004) 617–628, doi:10.1016/S0006-3495(04)74140-5.
[42] A.J. Engler, S. Sen, H.L. Sweeney, D.E. Discher, Matrix elasticity directs stem cell lineage specification, Cell. 126 (2006) 677–689, doi:10.1016/j.cell.2006.06.044.
[43] N. Zaari, P. Rajagopalan, S.K. Kim, A.J. Engler, J.Y. Wong, Photopolymerization in microfluidic gradient generators: microscale control of substrate compliance to manipulate cell response, Adv. Mater. 16 (2004) 2133–2137, doi:10.1002/adma.200400883.
[44] C.S. Chen, J.L. Alonso, E. Ostuni, G.M. Whitesides, D.E. Ingber, Cell shape provides global control of focal adhesion assembly, Biochem. Biophys. Res. Commun. 307 (2003) 355–361.
[45] S.J. Han, K.S. Bielawski, L.H. Ting, M.L. Rodriguez, N.J. Sniadecki, Decoupling substrate stiffness, spread area, and micropost density: a close spatial relationship between traction forces and focal adhesions, Biophys. J. 103 (2012) 640–648, doi:10.1016/j.bpj.2012.07.023.
[46] C.M. Lo, H.B. Wang, M. Dembo, Y.L. Wang, Cell movement is guided by the rigidity of the substrate, Biophys. J. 79 (2000) 144–152, doi:10.1016/S0006-3495(00)76279-5.
[47] S.I. Fraley, Y. Feng, A. Giri, G.D. Longmore, D. Wirtz, Dimensional and temporal controls of three-dimensional cell migration by zyxin and binding partners, Nat. Commun. 3 (2012) 719, doi:10.1038/ncomms1711.
[48] P.P. Girard, E.A. Cavalcanti-Adam, R. Kemkemer, J.P. Spatz, Cellular chemomechanics at interfaces: sensing, integration and response, Soft Matter 3 (2007) 307–326, doi:10.1039/B614008D.
[49] A. Müller, J. Meyer, T. Paumer, T. Pompe, Cytoskeletal transition in patterned cells correlates with interfacial energy model, Soft Matter 10 (2014) 2444–2452, doi:10.1039/c3sm52424h.
[50] Y.S. Choi, L.G. Vincent, A.R. Lee, K.C. Kretchmer, S. Chirasatitsin, M.K. Dobke, et al., The alignment and fusion assembly of adipose-derived stem cells on mechanically patterned matrices, Biomaterials 33 (2012) 6943–6951, doi:10.1016/j.biomaterials.2012.06.057.
[51] L.G. Vincent, Y.S. Choi, B. Alonso-Latorre, J.C. del Álamo, A.J. Engler, Mesenchymal stem cell durotaxis depends on substrate stiffness gradient strength, Biotechnol. J. 8 (2013) 472–484, doi:10.1002/biot.201200205.
[52] A.J. Engler, M.A. Griffin, S. Sen, C.G. Bönnemann, H.L. Sweeney, D.E. Discher, Myotubes differentiate optimally on substrates with tissue-like stiffness: pathological implications for soft or stiff microenvironments, J. Cell Biol. 166 (2004) 877–887, doi:10.1083/jcb.200405004.
[53] L.A. Flanagan, Y.-E. Ju, B. Marg, M. Osterfield, P.A. Janmey, Neurite branching on deformable substrates, Neuroreport 13 (2002) 2411–2415, doi:10.1097/01.wnr.0000048003.96487.97.

[54] O. Ilina, G.-J. Bakker, A. Vasaturo, R.M. Hofmann, P. Friedl, Two-photon laser-generated microtracks in 3D collagen lattices: principles of MMP-dependent and -independent collective cancer cell invasion, Phys. Biol. 8 (2011) 015010, doi:10.1088/1478-3975/8/1/015010.
[55] D. Irimia, G. Charras, N. Agrawal, T. Mitchison, M. Toner, Polar stimulation and constrained cell migration in microfluidic channels, Lab Chip. 7 (2007) 1783–1790, doi:10.1039/b710524j.
[56] M. Scianna, L. Preziosi, A cellular Potts model for the MMP-dependent and -independent cancer cell migration in matrix microtracks of different dimensions, Comput. Mech. 53 (2014) 485–497, doi:10.1007/s00466-013-0944-6.
[57] M. Scianna, L. Preziosi, Modeling the influence of nucleus elasticity on cell invasion in fiber networks and microchannels, J. Theor. Biol. 317 (2013) 394–406, doi:10.1016/j.jtbi.2012.11.003.
[58] A.L. Bauer, T.L. Jackson, Y. Jiang, A cell-based model exhibiting branching and anastomosis during tumor-induced angiogenesis, Biophys. J. 92 (2007) 3105–3121, doi:10.1529/biophysj.106.101501.
[59] B.M. Rubenstein, L.J. Kaufman, The role of extracellular matrix in glioma invasion: a Cellular Potts Model approach, Biophys. J. 95 (2008) 5661–5680, doi:10.1529/biophysj.108.140624.
[60] A. Shirinifard, J.S. Gens, B.L. Zaitlen, N.J. Popławski, M. Swat, J.A. Glazier, 3D multi-cell simulation of tumor growth and angiogenesis, PLoS One 4 (2009) e7190, doi:10.1371/journal.pone.0007190.
[61] S. Turner, J.A. Sherratt, Intercellular adhesion and cancer invasion: a discrete simulation using the extended Potts model, J. Theor. Biol. 216 (2002) 85–100, doi:10.1006/jtbi.2001.2522.
[62] D. Drasdo, G. Forgacs, Modeling the interplay of generic and genetic mechanisms in cleavage, blastulation, and gastrulation, Dev. Dyn. 219 (2000) 182–191, doi:10.1002/1097-0177(200010)219:2⟨182::AID-DVDY1040⟩3.0.CO;2-A.
[63] J. Moreira, A. Deutsch, Pigment pattern formation in zebrafish during late larval stages: a model based on local interactions, Dev. Dyn. 232 (2005) 33–42, doi:10.1002/dvdy.20199.
[64] T. Walther, H. Reinsch, A. Grosse, K. Ostermann, A. Deutsch, T. Bley, Mathematical modeling of regulatory mechanisms in yeast colony development, J. Theor. Biol. 229 (2004) 327–338, doi:10.1016/j.jtbi.2004.04.004.
[65] V.P. Zhdanov, B. Kasemo, Simulation of the growth and differentiation of stem cells on a heterogeneous scaffold, Physical Chemistry Chemical Physics 6 (2004) 4347–4350, doi:10.1039/b407371c.
[66] A.F.M. Marée, P. Hogeweg, How amoeboids self-organize into a fruiting body: multicellular coordination in *Dictyostelium discoideum*, Proc. Natl. Acad. Sci. USA 98 (2001) 3879–3883.
[67] N.J. Savill, J.A. Sherratt, Control of epidermal stem cell clusters by Notch-mediated lateral induction, Dev. Biol. 258 (2003) 141–153.
[68] A. Mochizuki, Pattern formation of the cone mosaic in the zebrafish retina: a cell rearrangement model, J. Theor. Biol. 215 (2002) 345–361, doi:10.1006/jtbi.2001.2508.
[69] P.K. Maini, L. Olsen, J.A. Sherratt, Mathematical models for cell–matrix interactions during dermal wound healing, Int. J. Bifurcation Chaos 12 (2002) 2021–2029, doi:10.1142/S0218127402005674.
[70] M. Scianna, An extended Cellular Potts Model analyzing a wound healing assay, Comput. Biol. Med. 62 (2015) 33–54, doi:10.1016/j.compbiomed.2015.04.009.
[71] N.J. Popławski, A. Shirinifard, M. Swat, J.A. Glazier, Simulation of single-species bacterial-biofilm growth using the Glazier–Graner–Hogeweg model and the Compucell3D modeling environment, Math. Biosci. Eng. 5 (2008) 355–388.
[72] R. Chaturvedi, C. Huang, J.A. Izaguirre, S.A. Newman, J.A. Glazier, M. Alber, P.M.A. Sloot, B. Chopard, A.G. Hoekstra, A hybrid discrete-continuum model for 3-D skeletogenesis of the vertebrate limb, Cellular Automata, Springer, Berlin, Heidelberg, 2004, pp. 543–552. http://link.springer.com/chapter/10.1007/978-3-540-30479-1_56 (accessed 29.07.15).
[73] R. Chaturvedi, C. Huang, B. Kazmierczak, T. Schneider, J.. Izaguirre, T. Glimm, et al., On multiscale approaches to three-dimensional modelling of morphogenesis, J. R. Soc. Interface 2 (2005) 237–253, doi:10.1098/rsif.2005.0033.
[74] N.J. Popławski, M. Swat, J.S. Gens, J.A. Glazier, Adhesion between cells, diffusion of growth factors, and elasticity of the AER produce the paddle shape of the chick limb, Physica A. 373 (2007) 521–532, doi:10.1016/j.physa.2006.05.028.
[75] C. Xue, A. Friedman, C.K. Sen, A mathematical model of ischemic cutaneous wounds, Proc. Natl. Acad. Sci. USA 106 (2009) 16782–16787, doi:10.1073/pnas.0909115106.
[76] Z. Xu, J. Lioi, J. Mu, M.M. Kamocka, X. Liu, D.Z. Chen, et al., A multiscale model of venous thrombus formation with surface-mediated control of blood coagulation cascade, Biophys. J. 98 (2010) 1723–1732, doi:10.1016/j.bpj.2009.12.4331.
[77] Z. Xu, N. Chen, M.M. Kamocka, E.D. Rosen, M. Alber, A multiscale model of thrombus development, J. R. Soc. Interface 5 (2008) 705–722, doi:10.1098/rsif.2007.1202.
[78] R.M.H. Merks, J.A. Glazier, Dynamic mechanisms of blood vessel growth, Nonlinearity 19 (2006) C1–C10, doi:10.1088/0951-7715/19/1/000.
[79] R.M.H. Merks, S.V. Brodsky, M.S. Goligorksy, S.A. Newman, J.A. Glazier, Cell elongation is key to in silico replication of in vitro vasculogenesis and subsequent remodeling, Dev. Biol. 289 (2006) 44–54, doi:10.1016/j.ydbio.2005.10.003.
[80] R.M.H. Merks, E.D. Perryn, A. Shirinifard, J.A. Glazier, Contact-inhibited chemotaxis in de novo and sprouting blood-vessel growth, PLoS Comput. Biol. (2008) 4, doi:10.1371/journal.pcbi.1000163.
[81] M. Scianna, L. Munaron, L. Preziosi, A multiscale hybrid approach for vasculogenesis and related potential blocking therapies, Prog. Biophys. Mol. Biol. 106 (2011) 450–462, doi:10.1016/j.pbiomolbio.2011.01.004.
[82] M. Scianna, A multiscale hybrid model for pro-angiogenic calcium signals in a vascular endothelial cell, Bull. Math. Biol. 74 (2012) 1253–1291, doi:10.1007/s11538-011-9695-8.
[83] A. Szabo, E.D. Perryn, A. Czirok, Network formation of tissue cells via preferential attraction to elongated structures, Phys. Rev. Lett. 98 (2007) 038102, doi:10.1103/PhysRevLett.98.038102.
[84] A. Szabó, R. Unnep, E. Méhes, W.O. Twal, W.S. Argraves, Y. Cao, et al., Collective cell motion in endothelial monolayers, Phys. Biol. 7 (2010) 046007, doi:10.1088/1478-3975/7/4/046007.
[85] A. Szabó, A. Czirók, The role of cell–cell adhesion in the formation of multicellular sprouts, Math. Model Nat. Phenom. 5 (2010) 106, doi:10.1051/mmnp/20105105.
[86] M. Scianna, R.M.H. Merks, L. Preziosi, E. Medico, Individual cell-based models of cell scatter of ARO and MLP-29 cells in response to hepatocyte growth factor, J. Theor. Biol. 260 (2009) 151–160, doi:10.1016/j.jtbi.2009.05.017.
[87] M. Scianna, L. Preziosi, K. Wolf, A Cellular Potts Model simulating cell migration on and in matrix environments, Math. Biosci. Eng. 10 (2013) 235–261.
[88] J. Starruß, T. Bley, L. Søgaard-Andersen, A. Deutsch, A new mechanism for collective migration in *Myxococcus xanthus*, J. Stat. Phys. 128 (2007) 269–286, doi:10.1007/s10955-007-9298-9.
[89] A.F.M. Marée, A. Jilkine, A. Dawes, V.A. Grieneisen, L. Edelstein-Keshet, Polarization and movement of keratocytes: a multiscale modelling approach, Bull. Math. Biol. 68 (2006) 1169–1211, doi:10.1007/s11538-006-9131-7.
[90] R.M.H. Merks, P. Koolwijk, Modeling morphogenesis *in silico* and *in vitro*: towards quantitative, predictive, cell-based modeling, Math. Model. Nat. Phenom. 4 (2009) 149–171, doi:10.1051/mmnp/20094406.
[91] M. Scianna, E. Bassino, L. Munaron, A cellular Potts model analyzing differentiated cell behavior during in vivo vascularization of a hypoxic tissue, Comput. Biol. Med. 63 (2015) 143–156, doi:10.1016/j.compbiomed.2015.05.020.